NASA TECHNICAL NOTE

NASA TN D-7810

NASA TN D-7810

TURBULENT HEAT-TRANSFER PREDICTION METHOD FOR APPLICATION TO SCRAMJET ENGINES

by S. Z. Pinckney

Langley Research Center
Hampton, Va. 23665

NATIONAL AERONAUTICS AND SPACE ADMINISTRATION • WASHINGTON, D. C. • NOVEMBER 1974

1. Report No. NASA TN D-7810	2. Government Accession No.	3. Recipient's Catalog No.
4. Title and Subtitle TURBULENT HEAT-TRANSFER PREDICTION METHOD FOR APPLICATION TO SCRAMJET ENGINES		5. Report Date November 1974 6. Performing Organization Code
7. Author(s) S. Z. Pinckney		8. Performing Organization Report No. L-9816 10. Work Unit No. 505-05-41-01
9. Performing Organization Name and Address NASA Langley Research Center Hampton, Va. 23665		11. Contract or Grant No. 13. Type of Report and Period Covered Technical Note
12. Sponsoring Agency Name and Address National Aeronautics and Space Administration Washington, D.C. 20546		14. Sponsoring Agency Code
15. Supplementary Notes		

16. Abstract In connection with a research program on hypersonic air-breathing propulsion, an integral method for predicting boundary-layer development in turbulent flow regions on two-dimensional or axisymmetric bodies has been developed through use of the integral-momentum, moment of momentum, and energy equations together with appropriate auxiliary equations. The method has the capability of approximating nonequilibrium velocity profiles as well as the local surface friction in the presence of a pressure gradient. An approach is developed to the problem of predicting the heat transfer in a turbulent boundary layer in the presence of a high pressure gradient. No provision was included to account for a pressure gradient normal to the surface. The solution was derived with particular emphasis on its applicability to supersonic combustion; thus, the effects of real gas flows were included. The resulting integrodifferential boundary-layer method permits the estimation of cooling requirements for scramjet engines. Theoretical heat-transfer results are compared with experimental combustor and noncombustor heat-transfer data and show reasonable agreement. The present heat-transfer method is used in the development of engine design concepts which, if utilized, will produce an engine with reduced cooling requirements. The Langley scramjet engine module was designed by utilizing these new design concepts and this engine design is discussed along with its corresponding cooling requirements. The present heat-transfer method is also used to develop a combustor cooling correlation for a combustor whose local properties are computed one-dimensionally by assuming a linear area variation and a given heat-release schedule.

17. Key Words (Suggested by Author(s))	18. Distribution Statement
Turbulent boundary layer Heat transfer Scramjet engines Combustor heat transfer	Unclassified – Unlimited STAR Category 12

19. Security Classif. (of this report)	20. Security Classif. (of this page)	21. No. of Pages	22. Price*
Unclassified	Unclassified	64	$4.25

*For sale by the National Technical Information Service, Springfield, Virginia 22151

TURBULENT HEAT-TRANSFER PREDICTION METHOD FOR APPLICATION TO SCRAMJET ENGINES

By S. Z. Pinckney
Langley Research Center

SUMMARY

In connection with a research program on hypersonic air-breathing propulsion, an integral method for predicting boundary-layer development in turbulent flow regions on two-dimensional or axisymmetric bodies has been developed through use of the integral-momentum, moment of momentum, and energy equations together with appropriate auxiliary equations. The method has the capability of approximating nonequilibrium velocity profiles as well as the local surface friction in the presence of a pressure gradient. An approach is developed to the problem of predicting the heat transfer in a turbulent boundary layer in the presence of a high pressure gradient. No provision was included to account for a pressure gradient normal to the surface. The solution was derived with particular emphasis on its applicability to supersonic combustion; thus, real gas flow effects were included. The resulting integrodifferential boundary-layer method permits the estimation of cooling requirements for scramjet engines.

Theoretical heat-transfer results are compared with experimental combustor and noncombustor heat-transfer data and show reasonable agreement. The theoretical heat-transfer method is used to predict heating and thus cooling requirements for a sample engine sized by estimates of vehicle drags at a range of altitudes and for Mach numbers of 6, 8, and 10. These calculations indicate that in hypersonic engine design, certain design concepts should be incorporated to account for the cooling requirements of the resulting engines. The general design concepts imposed on hypersonic engine design by engine cooling restrictions indicate that when engine cooling is considered, scramjets are advantageous at Mach numbers of about 6.0 and above, that combustor pressures should be kept at the minimum required for efficient combustion, and that the positive pressure gradients in the combustor should be kept as small as possible. Also these engine cooling restrictions require that combustor and nozzle wetted areas should be kept as small as possible; analysis of the sample engine indicates that the use of fuel injection struts provide a technique for reducing the ratio of combustor wetted area to combustor entrance area. The analysis of the sample engine also indicates that the operating Mach number range of an engine (relative to engine cooling requirements) can

be increased if the fuel injection is designed to keep the combustion in the center of the combustor and away from the surface.

The general design concepts imposed on engine design by engine cooling restrictions were utilized in the design of the Langley scramjet engine module. The resulting Langley scramjet engine module is discussed along with its corresponding cooling requirements.

The present heat-transfer method is used to develop a combustor or nozzle cooling requirement correlation for a combustor whose local flow properties throughout the combustor are computed one-dimensionally, a linear area variation and a given heat release schedule being assumed. This correlation can be used to obtain reasonable estimates of cooling requirements for a combustor of this type without a long calculation procedure.

INTRODUCTION

Generally, the engine selection for a particular flight application is based primarily on the specific impulse (ref. 1); however, results from an early analytical investigation on engine selection by Weber and MacKay (ref. 2) suggest that conclusions based on a single parameter could be misleading. In particular, Weber and MacKay suggest that the coolant requirements of a particular engine also may dictate the suitability of its use. For example, at hypersonic speeds the local heating rates of the subsonic burning ramjet could result in such large coolant requirements to maintain the integrity of the engine that the use of fuel as a coolant would not be practical. Even though at the chosen flight Mach number a lower specific impulse may be obtained with a scramjet than is obtained with a subsonic ramjet, the lower coolant requirements of the scramjet may necessitate its use. These considerations emphasize the importance of the cooling problem in engine selection and design and consequently, the ability to predict the heat transfer or thermal loading of an engine is a key factor.

The literature contains several detailed investigations of the engine coolant requirements of both subsonic burning ramjets and scramjets. (See refs. 2 to 4.) The heat-transfer predictions used to estimate the coolant requirements are generally based on methods employing the flat-plate Reynolds analogy type of heat-transfer predictions. (See refs. 5 to 7.) This method is inadequate where strong longitudinal pressure gradients exist, for instance, in the combustors of some ramjet and scramjet engines. Experimental evidence (refs. 8 and 9) show that heat-transfer rates in the presence of high positive pressure gradients are larger than those predicted by standard flat-plate Reynolds analogy methods, and experimental heat-transfer data measured in a supersonic combustor (ref. 10) reveal that particularly in combustors, much higher heat-

transfer rates may be generated by the higher turbulence levels than are predicted by these methods.

In order to be able to analyze heat transfer in high-speed compressible turbulent boundary layers with a pressure gradient, a scheme has to be developed which accounts for the effects of pressure gradient on all the significant parameters. (See ref. 11.) Considerable effort has been expended toward the prediction of the turbulent heat flux in flat-plate-type flows. Many of the better known modified Reynolds analogy type methods for flat-plate flows are summarized in references 7, 12, and 13. Generally, these methods were developed for use in turbulent boundary-layer integral-type techniques. (See, for example, refs. 14 to 17.) Several of the finite-difference type methods (for example, refs. 18 to 20) as well as some integral type techniques (for example, refs. 21 and 22) approach the turbulent heat-flux prediction through assumed relationships between the eddy viscosity and the eddy conductivity. These relationships are in the form of a turbulent Prandtl number and do not directly include any pressure gradient effects. In reference 11 Alber and Coats approach the problem of the prediction of the turbulent heat flux for incompressible flow through the use of an appropriate eddy conductivity model to determine a family of equilibrium enthalpy profiles. The resulting enthalpy profiles are generated in a manner similar to the approach that Mellor and Gibson (ref. 23) used in deducing the general family of incompressible equilibrium velocity profiles. Through use of these equilibrium enthalpy profiles, Reynolds analogy is shown to be a function of the longitudinal pressure gradient in incompressible flows. However, at present, the development of Alber and Coats (ref. 11) is applicable only to incompressible flows.

In the present report another approach is presented to the problem of predicting the heat flux in a compressible turbulent boundary layer in the presence of a large pressure gradient. The resulting solution was derived with particular emphasis on its application to supersonic combustion and to estimating the cooling requirements for scramjet engines. The method is based on the fact that a pressure gradient distorts the boundary-layer velocity profile and generates a level of turbulence which differs from that for a flat plate. Therefore, the local wall friction coefficient no longer is an adequate index to the wall heat transfer. In conjunction with this fact, the similarity in shape between a distorted nonequilibrium velocity profile and an equilibrium flat-plate velocity profile at either a lower or higher Reynolds number was observed. The success in heat-flux prediction for flat plates suggested the use, in the present method, of Reynolds analogy in combination with the friction coefficient corresponding to the equilibrium flat-plate velocity profile which is similar to the distorted or nonequilibrium profile. In a severe pressure gradient, this usage of friction coefficient can result in the use in Reynolds analogy of a friction coefficient which occurs at either a significantly lower or higher Reynolds number. Thus, the present method assumes that the corre-

sponding similar equilibrium flat-plate profile is associated with a level of turbulence which results in its friction coefficient being an adequate index to the wall heat flux of the actual boundary layer.

The basic integral method used is applicable to the prediction of axisymmetric and two-dimensional turbulent boundary layers and is similar to that of reference 14. The resulting method requires the simultaneous solution of the integral-momentum, moment of momentum, and energy equations. It includes the ability to approximate nonequilibrium boundary-layer velocity profiles and also includes the modified Crocco-type relation for the enthalpy-velocity profile relation of reference 24. The present boundary-layer prediction method is somewhat more complex than the version of reference 14 in that provisions for real gas (which can include combustion products) and nonisentropic boundary-layer edge conditions are included. The real-gas capability of the integral boundary-layer equations used in the prediction method includes terms which account for the change in combustion products in a boundary layer but do not include terms which actually compute the chemical reactions in the boundary layer. In addition, friction and heat-transfer coefficients are included which are functions of the local pressure gradients as well as the upstream history of the boundary layer. Several simplifying assumptions are retained such as a flat-plate shear stress profile and no provision for a normal pressure gradient or wall injection. The validity of the present method is determined by comparisons with the experimental heat-trasfer data of Hoydysh and Zakkay (ref. 25) and the experimental combustor heat-transfer data of Billig and Grenleski (ref. 10).

The present heat-transfer method is used to predict heating and thus cooling requirements for a sample engine sized by estimates of vehicle drags at a range of altitudes and for flight Mach numbers of 6, 8, and 10. The results of these engine-cooling predictions suggest that during engine design, certain design constraints should be imposed directly as a result of the cooling requirements of the engine. The Langley scramjet engine module was designed by using these engine cooling design constraints. The Langley scramjet engine module design is discussed along with the cooling requirements of the engine, and the effects of engine-cooling design constraints on engine performance.

The present heat-transfer method is also used to develop approximate correlation curves for making rapid estimates of cooling requirements for combustors. These correlations are based on theoretical heat-transfer calculations for a combustor designed for use on the Langley scramjet engine module. The combustor heat-transfer correlation assumes that the local flow properties throughout the combustor are computed one-dimensionally by assuming a linear area variation and a given heat release

schedule. These combustor heat-transfer correlations are based on analysis of full-scale combustors for flight Mach numbers of 6, 8, and 10 and for a range of altitudes.

SYMBOLS

A	area
A_c	combustor wetted area
A_v	constant in equation (7)
B	constant in equation (11)
C	function in equation (16) that depends on local integrated values of total energy and momentum deficiencies
C_f	local friction coefficient
c_p	specific heat at constant pressure
c_v	specific heat at constant volume
D	function defined in equation (2)
E	correlation function given by equation (13)
F	constant (= 2327) in equation (20)
$f\left(\frac{A_4}{A_3}\right)$	defined by equation (27)
G	gap between struts
H	flow height through engine
h	enthalpy
I	constant in boundary-layer equations ($I = 0$ for two-dimensional flow, $I = 1$ for axisymmetric flow)

I_{SP}	specific impulse
J	heat sink per kilogram of fuel
L	length of combustor
M	Mach number
N_{Pr}	Prandtl number as defined by equation (18)
n	number of combustor injection struts
p	static pressure
Q_f	heat sink in fuel for $\Phi = 1.0$
Q_Φ	integrated total heat transfer for fuel equivalence ratio burned, Φ
q_w	heat transfer to surface
q_∞	free-stream dynamic pressure
R_A	Reynolds analogy factor
R_θ	Reynolds number based on momentum thickness
r	body radius
T	temperature
u	velocity parallel to body surface and in direction of flow
v	velocity normal to body surface
W	flow width through engine
w	Coles' wake function
x	coordinate in free-stream direction

y	coordinate normal to body surface
Z	Karman factor
Γ	function defined by equation (23)
γ	ratio of specific heats, c_p/c_v
δ	boundary-layer thickness
δ^*	displacement thickness
θ	momentum thickness
κ	thermal conductivity (eq. (19))
λ	defined by equation (29)
μ	viscosity
ρ	density
τ	shear
Φ	fuel equivalence ratio burned
φ	energy thickness
ψ	defined by equation (28)
ω	angle between body surface coordinate and free-stream direction

Subscripts:

av	average
aw	adiabatic wall
I	inlet entrance

i	incompressible
L	local value
L.S.	value of parameter at laminar sublayer edge
max	maximum
pr	corresponding to the "similar" equilibrium flat-plate velocity profile
S.C.	determined from flat-plate Spalding-Chi friction method
t	stagnation value
w	wall value
δ	at the boundary-layer edge
θ	based on momentum thickness
∞	free stream
1	upstream body station
2	downstream body station
3	combustor entrance station
4	combustor exit station

ANALYTICAL METHOD

The present approach to the prediction of axisymmetric and two-dimensional turbulent boundary layers in the presence of heat transfer and a longitudinal pressure gradient utilizes a form of the integral boundary-layer equations that is similar to that derived in appendix A of reference 14. The continuity equation is combined with the momentum and energy equations and integrated across the boundary layer to produce integral forms for the momentum and energy equations. In addition, another integral equation is generated by multiplying the momentum equation by the normal distance from

the surface as a weighting function, combining the resulting equation with the continuity equation, and integrating across the boundary layer to form the integral moment-of-momentum equation. The assumptions are made that $v_w = 0$, $(dp/dy) = 0$, and the body radius is large relative to the boundary-layer thickness. The derivation of the integral boundary-layer equations of the present method differs from that of reference 14 in that the flow at the boundary-layer edge is not assumed to be isentropic. The integral equations are

Integral-momentum equation:

$$\frac{d\theta}{dx} + \theta\left(\frac{2 + \frac{\delta^*}{\theta}}{u_\delta}\frac{du_\delta}{dx} + \frac{1}{\rho_\delta}\frac{d\rho_\delta}{dx} + \frac{I}{r}\frac{dr}{dx}\right) - \left(\frac{1}{u_\delta}\frac{du_\delta}{dx} + \frac{1}{\rho_\delta u_\delta{}^2}\frac{dp_\delta}{dx}\right)\delta = \frac{1}{\cos\omega}\frac{\tau_w}{\rho_\delta u_\delta{}^2} = \frac{C_f}{2\cos\omega} \tag{1}$$

Integral moment-of-momentum equation:

$$\frac{\delta_2}{\delta_1} = e^D \tag{2}$$

where

$$D = \frac{1}{3}\left\{\frac{BC_f\,dx}{2\delta(B+1)\cos\omega\int_0^1 \frac{\rho u y}{\rho_\delta u_\delta \delta}\left(1 - \frac{u}{u_\delta}\right)d\frac{y}{\delta}} - d\log_e \rho_\delta u_\delta{}^2 - d\log_e \int_0^1 \frac{\rho u y}{\rho_\delta u_\delta \delta}\left(1 - \frac{u}{u_\delta}\right)d\frac{y}{\delta}\right.$$

$$- \frac{\int_0^1 \left[\left(1 - \frac{u}{u_\delta}\right)d\int_0^{y/\delta}\frac{\rho u}{\rho_\delta u_\delta}\,d\frac{y}{\delta}\right]d\frac{y}{\delta}}{\int_0^1 \frac{\rho u y}{\rho_\delta u_\delta \delta}\left(1 - \frac{u}{u_\delta}\right)d\frac{y}{\delta}} - \left(d\log_e \rho_\delta u_\delta\right.$$

$$\left. + I\,d\log_e r\right)\frac{\int_0^1 \left[\left(1 - \frac{u}{u_\delta}\right)\int_0^{y/\delta}\frac{\rho u}{\rho_\delta u_\delta}\,d\frac{y}{\delta}\right]d\frac{y}{\delta}}{\int_0^1 \frac{\rho u y}{\rho_\delta u_\delta \delta}\left(1 - \frac{u}{u_\delta}\right)d\frac{y}{\delta}} - I\,d\log_e r$$

$$\left. + \frac{\frac{1}{\rho_\delta u_\delta{}^2}dp_\delta + 2\left(\int_0^1 \frac{\rho u y}{\rho_\delta u_\delta \delta}\,d\frac{y}{\delta}\right)d\log_e u_\delta}{2\int_0^1 \frac{\rho u y}{\rho_\delta u_\delta \delta}\left(1 - \frac{u}{u_\delta}\right)d\frac{y}{\delta}}\right\}$$

Integral energy equation:

$$\frac{d\varphi}{dx} + \varphi \frac{d \log_e\left[\rho_\delta u_\delta (h_{t,\delta} - h_w) r^I\right]}{dx} = \frac{q_w}{\cos \omega \rho_\delta u_\delta (h_{t,\delta} - h_w)} \tag{3}$$

In equations (1) to (3), the following equalities are assumed:

$$\int_0^\delta \frac{\rho u}{\rho_\delta u_\delta}\left(1 - \frac{u}{u_\delta}\right) dy = \theta \tag{4}$$

$$\int_0^\delta \left(1 - \frac{\rho u}{\rho_\delta u_\delta}\right) dy = \delta^* \tag{5}$$

and

$$\int_0^\delta \frac{\rho u}{\rho_\delta u_\delta}\left(\frac{h_{t,\delta} - h_t}{h_{t,\delta} - h_w}\right) dy = \varphi \tag{6}$$

where the thermal-boundary-layer thickness is assumed to be equal to the velocity-boundary-layer thickness.

The turbulent boundary-layer predictions presented were generated through the simultaneous solution of equations (1) to (3). The present method requires values of θ, θ/δ, and φ at the initial station as input. The prediction then proceeds from this point to the end station of interest.

Auxiliary Relations for Turbulent-Boundary-Layer Solution

In order to obtain a simultaneous solution of equations (1) to (3) which is valid for turbulent boundary layers, auxiliary relations must be developed for the boundary-layer velocity profiles, the shear distribution across the boundary layer, local surface friction coefficient, the local surface heat transfer, and the boundary-layer enthalpy-velocity profile. In the present method, the flat-plate Spalding-Chi friction (based on R_θ, ref. 7) is utilized as a correlating parameter in the auxiliary relations developed for the boundary-layer velocity profile and for the shear distribution across the boundary layer. Also, through a modified version of the Reynolds analogy which is valid in pressure gradients, the flat-plate Spalding-Chi friction is utilized as a correlating parameter in the auxiliary relations developed for the local heat transfer and the boundary-layer enthalpy-velocity profile.

The velocity-profile relation given in equation (12) of reference 14 is assumed in the present method for use in the "law-of-the-wall" technique applied to the wake regions.

This relation is a modified version of the equilibrium flat-plate log semilog type velocity profile of reference 26; the modification permits an approximation of the pressure gradient effect on the velocity profile. The resulting velocity-profile relation is given by

$$\int_{u/u_\delta}^{1.0} \left(\frac{\rho}{\rho_\delta}\right)^{1/2} d\,\frac{u}{u_\delta} = 1.25\left(\frac{C_f}{2}\right)_{S.C.}^{1/2} \left(-A_V \log_e \frac{y}{\delta} + 2 - w\right) \tag{7}$$

The parameter w is Coles' wake function as given in reference 27. The parameter A_V is an unknown which must be determined by the solution of equations (1) to (3). The subscript S.C. means C_f is determined from the flat-plate Spalding-Chi friction method (based on R_θ). In a strong positive pressure gradient, A_V increases (fig. 1) and the actual surface C_f may decrease by several orders of magnitude. The use of the flat-plate friction in equation (7) instead of surface C_f tends to limit the spread of the calculated values of A_V and results in much shorter computer times required to iterate to an answer. For equilibrium flat-plate flow without heat transfer, the value of the parameter A_V as given in reference 26 is 2.0.

In the laminar sublayer region, a linear velocity profile is assumed from the wall to the edge of the laminar sublayer. For flat-plate flow the correlation of the laminar sublayer thickness (ref. 28) is given by

$$\left(\frac{y}{\delta}\right)_{L.S.} = \frac{26\,\frac{\mu_w}{\rho_w}}{\delta\left[\left(\frac{C_f}{2}\right)_{S.C.}\frac{\rho_\delta u_\delta^2}{\rho_w}\right]^{1/2}} \tag{8}$$

The laminar sublayer thickness as computed by equation (8) is believed to be controlled by the turbulence in the turbulent section of the velocity profile. For flat-plate flow, the friction coefficient $\left(C_f\right)_{S.C.}$ is an indirect measure of this turbulence. In a longitudinal pressure gradient, the turbulent section of the velocity profile is distorted compared with that of the equilibrium flat-plate velocity profile and thus the flat-plate friction coefficient $\left(C_f\right)_{S.C.}$ (based on local R_θ) is no longer a measure of the turbulence. Therefore, in order to utilize equation (8) to approximate the laminar sublayer thickness, another type of friction coefficient has to be used. The determination of the needed proportional friction coefficient resulted from the observation that there is a similarity in shape between a distorted nonequilibrium velocity profile and some equilibrium flat-plate velocity profiles. This observation suggested the use in equation (8) of the friction coefficient $\left(C_f\right)_{pr}$ corresponding to the equilibrium flat-plate velocity profile which is similar to the distorted or nonequilibrium profile. In a severe positive pressure gradi-

ent, this procedure results in the use of a friction coefficient which occurs at a significantly lower Reynolds number, whereas in a severe negative pressure gradient, this procedure results in the use of a friction coefficient which occurs at a much higher Reynolds number. Another reason why $\left(C_f\right)_{pr}$ should be a reasonable assumption to scale the turbulence in a highly distorted turbulent profile is indicated through the comparison of the shear distributions for the actual distorted profile and the similar equilibrium profile (fig. 2). The actual shear distribution across a turbulent boundary layer in a strong positive pressure gradient is shown in figure 2 to be zero at the boundary-layer edge, peak in toward the wall, and decrease to the wall shear values as the wall is approached. The shear distribution for the similar profile follows the shear distribution of the actual profiles until the peak shear is achieved and then continues on up to the value corresponding to $\left(C_f\right)_{pr}$ which is not much higher than the peak shear of the actual profile. Therefore, $\left(C_f\right)_{pr}$ is a good measure of the peak shear in the actual profile and thus the turbulence in the actual profile.

The flat-plate expression for the laminar sublayer thickness altered through use of the friction coefficient $\left(C_f\right)_{pr}$ which corresponds to the "similar" equilibrium flat-plate profile is given by

$$\left(\frac{y}{\delta}\right)_{L.S.} = \frac{26\,\frac{\mu_w}{\rho_w}}{\delta\left[\left(\frac{C_f}{2}\right)_{pr}\frac{\rho_\delta u_\delta^2}{\rho_w}\right]^{1/2}} \tag{9}$$

The expression for the friction coefficient $\left(C_f\right)_{pr}$ as given by

$$\left(C_f\right)_{pr} = \left[\frac{10A_v + \frac{dw}{d\left(\frac{y}{\delta}\right)}}{20 + \frac{dw}{d\left(\frac{y}{\delta}\right)}}\right]^2_{\frac{y}{\delta}=0.1} \left(C_f\right)_{S.C.} \tag{10}$$

is obtained by differentiating the "law-of-the-wall—law-of-the-wake" relationship of equation (7) with respect to y/δ first by using the equilibrium value of the parameter A_v and then second by using the value A_v determined from the solution of the governing equations. Since the local velocity profile is assumed to have the same shape as some equilibrium profile, $d\left(u/u_\delta\right)/d(y/\delta)$ for the two derivates can be set equal (in this case arbitrarily set at $(y/\delta) = 0.1$) and $\left(C_f\right)_{pr}$ of the equivalent equilibrium profile can be determined by using the resulting expression which is presented in equation (10).

(This friction coefficient $(C_f)_{pr}$ is used in Reynolds analogy to determine heat transfer.) Note that the resulting laminar sublayer thickness is the same as that for the similar equilibrium profile.

The relationship assumed for the shear distribution across the boundary layer is given in equation (14) of reference 14. This shear relationship was obtained by analytically fitting theoretical shear distributions derived (ref. 26) for flat-plate flow and is given by

$$\frac{\tau}{(\tau_w)_{S.C.}} = 1 - \left(\frac{y}{\delta}\right)^B \tag{11}$$

with

$$\frac{B}{B+1} = 0.08534 \log_e E + 0.7855 \tag{12}$$

where

$$E = M_\delta{}^2 \left(\frac{d\left\{ \frac{1}{\left(\frac{h}{h_\delta}\right)} \left[\frac{d\left(\frac{u}{u_\delta}\right)}{d\left(\frac{y}{\delta}\right)} \right]^2 \right\}}{d\left(\frac{y}{\delta}\right)} \right)_{\frac{y}{\delta}=0.95} \tag{13}$$

The correlation of the parameter B given by equations (12) and (13) is discussed in detail along with equation (11) in appendix B of reference 14. As pointed out in reference 14, the shear relation given in equation (11) has a maximum value at the surface and for all but severe pressure gradients the maximum shear does occur close to the surface and does not deviate much from that for a zero pressure gradient. (See ref. 29.) Therefore, for all but severe pressure gradient cases, accurate shear integrals are obtained even though equation (11) does not give the correct values of $(d\tau/dy)_w$ and τ_w for a pressure gradient situation. In the severe pressure gradients encountered in combustors, the accuracy of shear integrals predicted by using equation (11) is unknown but because of the lack of a better method for predicting the shear integral, the present turbulent boundary-layer prediction method uses equation (11).

In this analysis the friction coefficient used in the computation or the momentum losses is determined through use of equation (9) for the laminar sublayer thickness in conjunction with the predicted turbulent portion of the velocity profile (eq. (7)) and the relationship for the friction coefficient as given by (ref. 28)

$$C_f = \frac{2\left(\frac{u}{u_\delta}\right)^2_{L.S.}}{169\,\frac{\rho_\delta}{\rho_w}} \tag{14}$$

The laminar sublayer thickness is computed by substituting $\left(C_f\right)_{pr}$ in equation (9) which results in a laminar sublayer thickness equal to that of the similar equilibrium flat-plate velocity profile. The friction coefficient is than computed from the flat-plate expression given in equation (14) where $\left(u/u_\delta\right)_{L.S.}$ is the value of $\left(u/u_\delta\right)$ at $(y/\delta)_{L.S.}$ as obtained from the law-of-the-wall—law-of-the-wake relationship given in equation (7).

The heat transfer is computed by using the same form for the heat-transfer coefficient as that presented in reference 7 but with the input altered to account for the distortion of the boundary layer by a pressure gradient. The heat transfer to the wall is controlled by the turbulence in the boundary layer. For equilibrium flat-plate flow, the wall friction coefficient is a measure of this turbulence and thus the Reynolds analogy correlation. A pressure gradient can either enhance or retard the turbulence depending on the gradient. However, the boundary-layer velocity profile shape is still a measure of the turbulence (fig. 2) and thus $\left(C_f\right)_{pr}$ (of eq. (10)) of the similar equilibrium flat-plate profile is used in a modified Reynolds analogy to give for the heat transfer

$$\frac{q_w}{\rho_\delta u_\delta (h_{aw} - h_w)} = \frac{\left(C_f\right)_{pr}}{2Z} \tag{15}$$

The parameter Z in equation (15) is the Karman factor used in the modified Spalding-Chi heat-transfer method of reference 7 but $\left(C_f\right)_{pr}$ is used for the friction coefficient in the expression.

The enthalpy-velocity profile is assumed to be the modified Crocco-type relationship developed in reference 24 and given by

$$\frac{h}{h_\delta} = \frac{h_w}{h_\delta} + \left(1 - \frac{h_w}{h_\delta}\right)\left(\frac{u}{u_\delta}\right)^2 + \left[\frac{u}{u_\delta} - \left(\frac{u}{u_\delta}\right)^2\right]\frac{h_{aw} - h_w}{h_\delta}\frac{N_{Pr}}{Z} + C\left[\left(\frac{u}{u_\delta}\right)^2 - \left(\frac{u}{u_\delta}\right)^4\right] \tag{16}$$

The parameter C is an unknown that has to be determined by the solution of the governing equations and is a function of the local integrated total-energy and momentum deficiencies. With the use of equation (16), integration of the boundary-layer profile produces an energy deficiency equal to the upstream body surface heat transfer. For use in the surface heat-transfer relation of equation (15) and the enthalpy-velocity profile relation of equation (16), the adiabatic wall enthalpy was assumed to be of the form

$$h_{aw} = h_\delta + N_{Pr}^{1/3} \frac{u_\delta^2}{2} \tag{17}$$

where the Prandtl number is given by

$$N_{Pr} = \frac{c_p \mu}{\kappa} = \frac{4\gamma}{9\gamma - 5} \tag{18}$$

The relation for the Prandtl number given in equation (18) is a result of the relationship for the thermal conductivity of real air or a real gas presented in reference 30 and given by

$$\kappa = 0.25(9\gamma - 5)\mu c_v \tag{19}$$

Analytical Method of Solution

Substitution of the turbulent auxiliary relations into equations (1) to (3) produces three ordinary integral differential equations with three unknowns. As in reference 14, the unknowns consist of the parameter A_v of the velocity profile, the parameter C of the temperature-velocity profile, and the longitudinal boundary-layer thickness change. The parameters that are required as input at the initial station are the momentum thickness, the ratio of momentum to boundary-layer thickness, and the energy thickness. In addition to the three parameters at the initial station that have been mentioned, additional input consisting of pertinent boundary-layer edge and surface conditions is needed. For turbulent boundary-layer predictions in real air, empirical correlations of h_w, h_δ, ρ_δ, and u_δ corresponding to the real air tables of reference 31 were obtained and are given by

$$h = \left[\left(\frac{9}{5}\right)^2 (0.00001277)T^2 + \frac{9}{5}(0.2262)T\right]F \tag{20}$$

where T is in degrees Kelvin, F is equal to 2327, and h is in joules per kilogram.

$$\rho_\delta = 0.00251 \frac{p_\delta}{2117}\left[\frac{3.447}{\left(\frac{h_\delta \frac{1}{F}}{33.7098}\right)^{0.992}} + 0.00555\left(\frac{h_\delta \frac{1}{F}}{33.7098}\right)^{0.4014} - 0.00672\right]\frac{515.379}{47.8803} \tag{21}$$

where p_δ is in newtons per meter squared, h_δ is joules per kilogram, and ρ_δ is in kilograms per meter cubed.

$$u_\delta = (1087.4)(0.3048)\left[0.5368\left(\frac{h_\delta \frac{1}{F}}{33.7098}\right)^{0.4888} - 0.002005\left(\left|\frac{h_\delta \frac{1}{F}}{33.7098} - 5\right|\right)^{1.479} + 0.01557\right.$$

$$\left. - \frac{1.716}{10^{11}}\left(\left|\frac{h_\delta \frac{1}{F}}{33.7098} - 5\right|\right)^{5.73}\right] M_\delta \tag{22}$$

where h_δ is in joules per kilogram and u_δ is in meters per second. Thus, for real air, input distributions of T_w, T_δ, p_δ, and M_δ are needed in conjunction with γ_δ, γ_w, and geometric inputs.

In a combustor or nozzle region, inputs of T_w, h_w, T_δ, h_δ, u_δ, M_δ, p_δ, γ_δ, γ_w, and ρ_δ are needed as input in the computer program in conjunction with geometric inputs. These relevant boundary-layer edge parameters in the combustor or nozzle regions are generated through use of a one-dimensional combustor design computer program developed for supersonic combustion with hydrogen as the fuel. The computer program for calculating the static pressure and other flow parameter distributions in a one-dimensional supersonic combustor channel was developed at NASA Langley Research Center. Real-gas thermodynamic properties for mixtures of hydrogen and air reacted to a specified degree are used for the calculations. Input to the program includes the entering fuel and air states, the channel geometry, and the distribution of fuel injection and fuel reaction with distance along the channel. Output consists of the state at each point calculated along the channel, and line printer plots of selected parameter variations with distance. This computer program is available from Computer Software Management and Information Center, The University of Georgia, Athens, Georgia 30601 under the computer program number LAR-11041.

In the simultaneous solution of equations (1) to (3), the enthalpy distribution across the boundary layer is obtained by use of equation (16). A relationship between the local density and local enthalpy in the turbulent boundary layer is assumed to be similar to that of the perfect-gas equation of state

$$\rho = \frac{\Gamma}{\Gamma - 1}\frac{p}{h} \tag{23}$$

In the boundary-layer solution the coefficient of equation (23) $\Gamma/(\Gamma - 1)$ is assumed to vary across the boundary layer from the wall value to the stream value in proportion to the local boundary-layer velocity

$$\frac{\Gamma}{\Gamma - 1} = \left(\frac{\Gamma}{\Gamma - 1}\right)_w + \frac{u}{u_\delta}\left[\left(\frac{\Gamma}{\Gamma - 1}\right)_\delta - \left(\frac{\Gamma}{\Gamma - 1}\right)_w\right] \tag{24}$$

This assumption is not exact but gives high accuracy over most of δ. The value of Γ_δ at the boundary-layer edge is determined with the computer program from

$$\Gamma_\delta = \frac{\rho_\delta h_\delta}{\rho_\delta h_\delta - p_\delta} \tag{25}$$

Simply, the solution of equations (1) to (3) across a body surface element consists of obtaining a first approximation of the values of A_v, C, and δ_2/δ_1 at the downstream body station of the element by use of the known parameters at the upstream station. Then, by using successive approximations of the downstream body stations, values of the parameters A_v, C, and δ_2/δ_1 yield successively better average values over the element of the integral parameters δ^*, θ, and μ. With the resubstitution of the revised values of the integral parameters into equations (1) to (3), successively better approximations of the parameters A_v, C, and δ_2/δ_1 are obtained. This method of successive approximations is continued until two successive calculations produce a change in the downstream value of δ^* of 1 percent or less.

More specifically, the actual solution of equations (1) to (3) across a body element consists of first converting all derivatives in equations (1) to (3) to finite changes across a body element. Upon doing this, expressions for the change in momentum thickness θ, change in energy thickness φ, and the boundary-layer thickness ratio across a body element are obtained from equations (1) to (3). These expressions are in terms of boundary-layer edge parameters, body surface parameters, body geometry, and integral parameters for the two body stations. The integral parameters include all the boundary-layer profile parameters such as u/u_δ, h/h_δ, ρ/ρ_δ, and τ/τ_w. The body geometry, all the boundary-layer edge conditions, and all the body surface conditions except the surface heat transfer and friction are inputs to the computer program or computed in the program. The surface heat transfer and friction are functions of the velocity profile as given in equations (9), (10), (14), and (15). The boundary-layer density profile is related to the enthalpy profile in the manner given by equation (23) and the boundary-layer shear profile is a function of the velocity and enthalpy profiles as given in equations (11) to (13). Therefore, the solution to the expressions for momentum and energy thickness change and the boundary-layer thickness ratio across a body element becomes the problem of approximating the boundary-layer velocity and enthalpy profiles for the two body stations. At any body station the boundary-layer velocity and enthalpy profiles are completely defined if the values of the unknowns A_v and C are known for that body station. For the upstream body station, the values of δ, θ, and φ are known either from the input to the program if it is the initial body station or the values have been computed in the program. If the values of δ, θ, and φ for any body station are known, the velocity and enthalpy profiles and therefore A_v and C are determined in the following manner. Assume two values of A_v for the body station. For each

value of A_V iterate on an unknown C of equation (16) by computing successive values of θ/δ and φ/δ from equations (4) and (6) until the values of δ are the same when computed from θ/δ or φ/δ by using the known values of θ and φ. By use of the results computed for each of the assumed values of A_V, iterate on A_V until the computed value of δ matches the known value of δ for the body station. For the first approximations of momentum and energy thickness change and boundary-layer thickness ratio across the body element, the known velocity and enthalpy profiles for the upstream body station are input for both body stations. If the values of δ, θ, and φ for the upstream body station are known, the first approximations for δ, θ, and φ for the downstream body station can then be computed. From use of the procedure already discussed for obtaining the boundary-layer velocity and enthalpy profiles when δ, θ, and φ are known, the first approximation for the downstream body stations of the pertinent parameters and profiles can be computed. This procedure is repeated except with successively better downstream body station parameters and profiles being used in the expressions for momentum and energy thickness change and boundary-layer thickness ratio across a body element. Successive approximations are computed until two successive calculations produce a change in the predicted value for the downstream body stations for δ^* of 1 percent or less.

COMPARISONS OF THEORY WITH EXPERIMENTAL DATA

The validity of the basic integral technique of the present method is demonstrated in reference 14 where experimental and theoretical distributions of δ, δ^*, and θ are compared over broad Mach number, Reynolds number, and wall temperature ranges. The conclusion is drawn that the method will predict these parameters within the limits of experimental accuracy. Therefore, the validity of the newly developed modified Reynolds analogy type heat-transfer method of the present paper remains to be determined by the comparison of theoretical heat-transfer predictions with experimental heat-transfer data. For flat-plate flow, the present heat-transfer prediction method reduces to the commonly accepted, modified flat-plate Reynolds analogy method of reference 7. Therefore, the comparisons of theoretical and experimental heat transfers presented in the present paper are restricted to flows with a pressure gradient and the data were taken from references 10 and 25.

Polynomial Flare Data

The configuration of reference 25 was an axisymmetric 42° turning angle polynomial flare and the results are presented in figure 3. The experimental boundary layer had a large normal pressure gradient. Because the present method does not provide for a normal pressure gradient, the corresponding theoretical heat-transfer calculations

were based on wall static pressures. Also presented in figure 3 is a theoretical heat-transfer distribution computed by use of the method of reference 32, which assumes that the turbulent and laminar Prandtl numbers are 1.0. It was surprising that both methods predicted almost identical heat-transfer results although a severe longitudinal pressure gradient appeared to be present. Examination of the velocity profiles predicted by the present method revealed essentially no velocity profile distortion from equilibrium flat-plate flow. In figure 4 experimental velocity profiles are compared with a representative theoretical velocity profile; the theoretical velocity profiles computed for all cases lie within ±0.015 (in u/u_δ) of the one given in figure 4. A typical velocity profile distorted by a strong positive pressure gradient is also given in figure 4. The values of u_δ and δ used to nondimensionalize the experimental data differ from those of the theoretical calculations by as much as 5 percent and 24 percent, respectively. Therefore, the experimental data were nondimensionalized by the same u_δ and δ as that of the theoretical predictions and essentially the same conclusion as to whether the velocity profile distortion occurs resulted. It is concluded that the experimental velocity profiles do not deviate much from those obtained for equilibrium flat-plate flow and that the use of the surface static pressures to determine boundary-layer edge parameters produced accurate predictions of the heat transfer, as indicated in figure 3.

Supersonic Combustor Data

The heat-transfer data of reference 10 were taken by use of the combustor configuration presented in figure 5. The combustor consists of an initial constant-area section followed by a conical section. The fuel is injected from eight orifices equally spaced around the combustor entrance. The combustor entrance conditions are approximately a Mach number of 3.2, a static pressure of 53.2 kN/m^2, and a static temperature of 780 K. But in order to compute local heat-transfer rates, distributions of p_δ, ρ_δ, u_δ, h_δ, h_w, γ_w, and γ_δ are needed as input to the computer program. In order to obtain these input parameters, a combustion heat-release rate and a combustion length are needed as input into the computer program which is used for supersonic combustor parameter calculations.

The quantity of fuel injected in the combustor of reference 10 resulted in an overall equivalence ratio of 0.5. Reference 10 states that most of the heat release occurred within the constant area section of the combustor. On the basis of this information, two cases have been computed that correspond to one-dimensional flow, an approximately constant heat release rate along the combustor, and overall combustion lengths extending from the injector station to x-stations of 0.25 meter (case 1) and 0.325 meter (case 2). The resulting values of boundary-layer edge flow parameters are given in figure 6. A comparison of these two cases with the experimental wall static pressure

and heat-transfer distributions should provide an indication of the effects of the length assumption.

In addition to the length parameter the assumption of one-dimensional flow was explored because the combustion probably did not occur uniformly across the duct. For instance, the penetration and mixing data of reference 33 indicate that the fuel would not reach the center line of the combustor within the constant-area section. It is possible that most of the fuel burned to an equivalence ratio of close to 1.0 near the wall of the combustor within the constant-area length and then the combustion products mixed with the core flow further downstream. Therefore, a third case was computed in which the combustion at the edge of the boundary layer reached an equivalence ratio of 1.0 at an x-station of 0.325 meter; downstream of this point it was assumed that mixing occurred and reduced the equivalence ratio to ≈ 0.5 at an x-station of 0.55 meter. In this case iterations of area were performed in the solution for the boundary-layer edge parameters resulting from the combustion process (see fig. 7) in order to produce a longitudinal pressure distribution approximating a faired curve through the experimental data shown in figure 8.

The longitudinal static-pressure distributions for the three cases are compared with the experimental data in figure 8. The data points in the constant-area region where the combustion occurred indicate three-dimensional flow effects presumably caused by discrete shock and expansion waves whereas the flow analysis is one-dimensional. In the expanding area duct downstream of the x-station of 0.325 meter, both cases 1 and 2 overpredict the experimental static pressure by about 20 percent. As noted above for case 3, a pressure distribution close to the experimental data was used.

A comparison of the theoretical and experimental heat-transfer distributions is given in figure 9. Up to the station corresponding to an x value of 0.4 meter, case 2 again agrees with the data better than case 1; however, case 3 provides the closest agreement. Beyond this station none of the three theoretical curves produced a slope which agreed with the data curve. This lack of agreement relative to slope is related to how quickly the distorted boundary layer reverts to a flat-plate type profile in a negative pressure gradient, which, in turn, is controlled by the shear distribution relations of equations (11) to (13).

Although the theoretical predictions of figure 9 deviated in various local details from the data, it should be noted that the integrated total heat transfer for the three cases differed from the integration of the data curve by a maximum of only 4 percent. In contrast the integrated value for the reference flat-plate curve is only 52 percent of the experimental value. Reference 10 also gives a total heat-transfer value determined from a heat balance on the coolant fluid of 0.583 MW, which is 89 percent of the integra-

tion of the local experimental values. The maximum spread between total heat-transfer values for the three theoretical cases and the two experimental values is 13 percent and the theory is concluded to be a satisfactory design tool.

ENGINE DESIGN FEATURES FOR REDUCED COOLING

A principal goal of the research program on integrated scramjet concepts at the NASA Langley Research Center is the development of designs with an engine-cooling requirement equivalent to only a fraction of the total fuel heat sink available. This goal will provide the vehicle designer with a much broader range of approaches since he will be able to use the excess heat sink for actively cooled vehicle structures and avoid many of the problems of hot structures and the associated aerodynamic disadvantages. (See refs. 34 to 36.)

The Langley program has resulted in the definition of a concept for an integrated scramjet module, an early version of which is described in references 35 to 37 and shown in figure 10. The engine concept is fixed geometry with sweptback sidewall compression surfaces. An open area is provided upstream of the cowl leading edge for flow spillage in the downward direction during inlet starting and low-speed operation. The three fuel injection struts are swept at the same angle as the sidewall leading edges since constant flow properties would tend to exist in planes parallel to the sweep. The front halves of the struts contribute to the compression of the inlet flow and the rear half contains installations of discrete fuel injector orifices. The expanding area combustor permits operation over a wide Mach number range without thermal choking. Part of the exhaust nozzle is included in the module; however, the aft end of the vehicle would be used to expand the exhaust further. A new version of the engine was developed on the basis of the results of extensive design studies in all areas, including general cooling analyses which employed the present prediction technique and are described in the following sections. These analyses were directed at evaluating the two principal methods for reducing engine cooling load: the reduction of wetted area, and the reduction of heat-transfer coefficient.

Reduced Combustor Wetted Area

The scramjet combustor generally is subjected to higher levels of pressure and temperature than the other engine components; therefore, it has the highest cooling loads and particular attention to the design features is required. The wetted area can be reduced if the length required for efficient combustion can be reduced. Since the kinetic effects (ignition and reaction lengths) generally are second order, the problem is reduced to minimizing the fuel-air mixing lengths. Mixing length is proportional to the spacing between adjacent fuel jets; therefore, fuel injection is desired from many

points in the stream by use of some device such as fuel injection struts. This effect is illustrated in figure 11 where combustor wetted area A_c expressed as a ratio to the combustor entrance area A_3 is given as a function of the number n of fuel injection struts. The mixing or combustor length L is assumed to be proportional to the gap G between the struts and the total cross-sectional area of the struts is assumed to be constant in order to handle the required fuel flow internally. With these assumptions the combustor wall wetted area tends to be inversely proportional to n + 1; however, the strut wetted area is directly proportional to $\sqrt{\frac{n}{n+1}}$. Therefore, the total wetted area approaches a minimum value greater than zero as n increases. An installation with three struts clearly has realized most of this technique without requiring an impractically large number of struts. Another obvious technique for reducing combustor wetted area is to develop configurations with cross sections which approach a circular or square shape.

Reduced Heat-Transfer Levels

The combustor design and operating conditions can be made to favor the maintenance of lower pressure levels in the combustor, generally with some sacrifice in thrust; therefore, a trade-off can be made between performance and cooling requirements. At a flight Mach number of 6.0, for instance, the scramjet can be designed to operate with either subsonic or supersonic combustion; however, supersonic combustion generally will produce lower pressures in the combustor and less heat transfer. These effects are illustrated in figure 12, which presents the results of a Mach 6 flight analysis for an altitude of 34 200 m (112 000 ft) and an equivalence ratio of 1.0. Flow conditions along the surfaces of the inlet (fig. 10) were determined by use of real-gas, swept, planar shock theory. The flow conditions in the rest of the engine were determined by using conventional one-dimensional thermodynamic engine cycle analyses. The subsonic combustion case clearly requires nearly three times the cooling for supersonic combustion because the static pressure near the combustor entrance is nearly four times as high. Since the use of supersonic combustion would reduce the specific impulse by only 8 percent, the trade-off is very favorable toward reduced cooling.

Scramjet combustors normally are designed with an expanding flow area in order to avoid thermal choking at the low end of the speed range. The rate of expansion and overall area ratio in the combustor are prime factors in determining the pressure levels and heat-transfer rates. This effect is illustrated by the results of figure 13 for a Mach 8 flight analysis for a cruise condition corresponding to an equivalence ratio of 0.75 and an altitude of 37 500 m (123 000 ft). The larger area ratio of the combustor (A_4/A_3 of 2.5) resulted in a 30-percent reduction in cooling requirement with a 4-percent loss in specific impulse, again, a very favorable trade-off. This method of reducing

cooling load has been evaluated with a more sophisticated combustor analysis for a Mach 10 case described in reference 34 where a 20-percent reduction in heat load was predicted for only a 3-percent loss in specific impulse.

The combustor cooling load also can be reduced by avoiding adverse pressure gradients in the combustor, as noted in the discussion of the present analytical method. Ideally, the engine inlet should provide the desired amount of compression, and combustion should occur at constant pressure. This goal is difficult to achieve for designs where a wide operating range of flight Mach number is required; however, it may be approached by matching as closely as possible the fuel injector design, location, and operation to combustor design and flight conditions. (See ref. 34.) The parameter A_V, defined in equation (7), provides a measure of the effect of pressure gradient on the distortion of the boundary-layer velocity distribution and therefore the heat transfer. Typical values of A_V are given in figure 1 for both mild and large positive pressure gradients. Another section of the paper shows that heat transfer is proportional to A_V^2; therefore, the virtue of keeping A_V small by designing for constant pressure combustion is clear.

Another effective method for reducing the heat-transfer coefficient is to shield the combustor walls from the high-enthalpy combustion products. With a fuel injector strut arrangement similar to that of figure 10, it should be possible to design the injectors so that the heat release in the layer of air next to the walls is delayed until the flow is near the combustor exit. This type of design should be particularly feasible for cruise conditions where the equivalence ratio is less than 1.0. The results of an analysis evaluating this effect are given in figure 14 for an equivalence ratio of 0.75. The lower curve assumes that the heat load on the inlet and combustor walls corresponds to the flight stagnation enthalpy and therefore the walls up to the combustor exit are not exposed to combustion enthalpies. This technique could reduce the engine cooling load by amounts up to 35 percent at Mach 10.

COOLING REQUIREMENTS FOR LANGLEY SCRAMJET MODULE

The configuration of the Langley engine shown in figure 10 has been modified and refined as a result of additional design studies and experimental work in the inlet and combustor areas. The revised design, as shown in figure 15, is described in detail in reference 34. The cooling requirements have been estimated by using the present prediction method for a Mach number range from 4 to 10, an equivalence ratio of 1.0, and a free-stream dynamic pressure of 47.9 kN/m^2 (1000 lb/ft^2). A vehicle with a take-off gross weight of 455 000 kg (10^6 lb) was assumed, and the engine module inlet was located 55 meters (180 ft) downstream of the nose of the vehicle. The inlet was

2.44 meters high by 1.95 meters wide (8 by 6.4 ft). The boundary layer developed on the lower surface of the vehicle forebody was ingested by the inlet. For simplicity, the turning through the vehicle bow shock was assumed to be constant at 8^{o}. The nozzle extended along the vehicle afterbody to a point where the effective exit area was 2.84 times the cowl capture area. Other assumptions and input to the analysis are discussed in the following paragraphs together with the results.

Inviscid flow analyses were conducted to determine the boundary-layer edge conditions. Inlet shock diagrams were constructed by using the real-gas swept shock theory. Examples are given in figures 16(a) and 16(b) for Mach numbers of 6.07 and 9.22, respectively. For the upper surface and cowl, a representative path was selected in these diagrams, and the conditions along this path were applied across the width of the inlet. The flow conditions in the combustor were predicted by using the one-dimensional theory for specified mixing and reaction distributions with length as discussed in reference 34. Flow conditions throughout the nozzle were computed by use of a conventional two-dimensional real-gas characteristics method.

Some of the results of these analyses are given in figure 17 which presents the boundary-layer edge Mach number and static pressure and temperature distributions along the top surface of the engine for two flight Mach numbers. The positions of the entrance and exit of the combustor are indicated. The Mach number drops a small amount near the combustor entrance and then remains nearly constant throughout the rest of the combustor length. This type of distribution is a result of the design concept, which utilizes a combination of normal and axial fuel injection which produces a heat-release schedule which closely matches the combustor geometry. (See ref. 34.) The net result is a generally decreasing static pressure along the combustor which is favorable to lower heat-transfer coefficients, as discussed previously. The heat release in the combustor produces substantial increases in the static temperature, which in the one-dimensional theory is uniformly distributed across the combustor. Heat release is inherent with combustion and its effect on heat load has to be minimized by other factors, such as designing for short combustors with low wetted area. It is of interest to note that even with the rather modest inlet contraction ratios of the Langley scramjet design, very substantial adverse pressure gradients occur in the downstream end of the inlet.

Some of the results of the analysis of the top surface are given in figures 18 and 19 in terms of distributions of the boundary-layer displacement and momentum thicknesses, and wall friction and heat-transfer coefficients. Initial values at station zero represent the results of the boundary-layer analysis for the forebody of the vehicle. At the entrance to the inlet the ratios of δ^*/H_I and δ/H_I are approximately 0.05 and 0.12, respectively. The values of δ^* and θ decrease in general in the combustor because the periphery or width increases in the expanding area channel. The value of the fric-

tion coefficient increases substantially along the combustor and upstream end of the nozzle primarily because the Reynolds number decreases by over an order of magnitude. However, when these effects are combined with the rapidly shrinking values of mass flow per unit area in the expanding area channel, the heat-transfer coefficient reaches a peak value near the combustor entrance and decreases rapidly thereafter; this effect prevents the cooling requirement from becoming excessive.

Heat-transfer coefficients were determined for all four walls of the engine and were applied to the wetted surface areas given in figure 20, which also presents values for a typical axisymmetric pod for comparison. The rectangular inlet of the Langley scramjet has three times the wetted area of the axisymmetric inlet; however, since the heat-transfer coefficients in the inlet are low, this is not a serious problem. The combustor, which does have high heat transfer, has much less wetted area than the axisymmetric configuration, and this is one of the primary reasons for the low cooling requirements of the Langley engine. The total wetted area of the Langley module is approximately equal to the podded engine; however, for the integrated module installation a substantial amount of surface area, which is external to the module and on the vehicle afterbody, is wetted by the engine exhaust. In the present analysis this area has been considered to be part of the engine; however, the heat-transfer coefficients are low over most of this region (x values greater than 20 meters in fig. 19) and regenerative cooling might not be required.

The overall results of the analysis are given in figure 21 in terms of the total cooling required for each engine component relative to the heat sink available in the fuel. For comparison purposes the total engine cooling requirement for the typical axisymmetric pod engine is presented in figure 21 for a Mach number of 6.0. For the Langley scramjet module excess heat sink is available over the entire Mach number range considered. It is clear that the nozzle, which includes the vehicle afterbody, is responsible for about one-half of the total engine cooling requirement. As discussed in reference 34, the nozzle design is very conservative and investigations are now in progress which are aimed at reducing the nozzle length and wetted area by as much as 50 percent. The solid curves of figure 21 correspond to an assumption of a constant wall temperature of 1110 K (2000° R). Realistically, this condition is not possible with current fuel circuit design technology; therefore, the effect of this assumption was tested by postulating a variable wall temperature. An arbitrary temperature distribution ranging from a value of 330 K near the leading edges of the inlet to a high of 1110 K in the combustor to 500 K at the end of the nozzle was assumed. As noted in figure 21, the net effect at the high end of the Mach number range was to increase the total cooling by only about 15 percent.

CORRELATION OF THE COMBUSTOR COOLING FOR A HYDROGEN FUELED SCRAMJET

The use of the present heat-transfer method to predict the combustor cooling requirements of a scramjet engine results in a long complicated calculation procedure. Thus, with a known engine, the use of the method to obtain combustor cooling requirements within a short time becomes paractically impossible. Therefore, because of the favorable comparisons of experimental and theoretical integrated total heat transfers (fig. 7), and also because of the relatively large range and quantity of theoretical combustor integrated total heat-transfer computations that have been made (table I), it was decided to use combustor heat-transfer results from the present heat-transfer method in an attempt to generate a theoretical correlation.

The desired combustor cooling correlation, as determined from dimensional analysis (details are presented in appendix), is given by the following relationship between the various combustor flow parameters and combustor geometric characteristics:

$$\left(\frac{Q_\Phi}{Q_f}\right)\frac{(\rho u)_I\left(q_\infty A_I^{1/2}\right)^{1/7}\left(1+\frac{\gamma-1}{2}M_\infty^{\,2}\right)\frac{4}{A_V^{\,2}}J}{\left[\rho_\delta u_\delta\left(h_{t,\delta}-h_w\right)\right]_3} \propto \frac{\Phi A_c}{A_I}\,f\left(\frac{A_4}{A_3}\right) \tag{26}$$

where

$$f\left(\frac{A_4}{A_3}\right)=\frac{4}{\frac{A_4}{A_3}}\,\frac{1-2\left(\frac{A_3}{A_4}\right)^{1/2}+\frac{A_3}{A_4}}{1-2\,\frac{A_3}{A_4}+\left(\frac{A_3}{A_4}\right)^2} \tag{27}$$

By using the proportionality presented in equation (26), a theoretical correlation has been generated for the combustor cooling predictions for scramjet engines with hydrogen combustion and is presented in figure 22. In figure 22 the ordinate ψ as given by the left-hand side of the proportionality expressed in equation (26) is

$$\psi=\frac{Q_\Phi}{Q_f}\,\frac{(\rho u)_I\left(q_\infty A_I^{1/2}\right)^{1/7}\left(1+\frac{\gamma-1}{2}M_\infty^{\,2}\right)\frac{4}{A_V^{\,2}}J}{\left[\rho_\delta u_\delta\left(h_{t,\delta}-h_w\right)\right]_3} \tag{28}$$

In figure 22 the abscissa λ as given by the right-hand side of proportionality expressed in equation (26) is

$$\lambda = \frac{\Phi A_c}{A_I} f\left(\frac{A_4}{A_3}\right) \tag{29}$$

The range of engine parameters for which combustor coolant requirements were determined for use in the generation of the correlation curves of figure 22 is given in table I. The theoretical heat-transfer results of table I were generated by using the present heat-transfer method; the local combustor parameters were computed one-dimensionally by assuming a linear combustor area variation in conjunction with a heat-release schedule. The effect of different heat-release assumptions on combustor cooling requirements is also demonstrated in figure 22 by two correlations, one for fuel injections normal to the stream (open symbols) and the other for fuel injections parallel to the stream (closed symbols). In figure 22 (and thus table I), the theoretical points corresponding to $q_\infty = 16.8$ kN/m^2 were computed by using heat-release schedules similar to those observed for normal injection whereas the theoretical points corresponding to $q_\infty = 47.8$ kN/m^2 were computed by using heat-release schedules generated from mixing correlations discussed in reference 34. In the range of geometry and flow parameters covered, a reasonable correlation is obtained.

In order to utilize the theoretical correlation of figure 22 to estimate the cooling requirements of a combustor, four pieces of information are needed other than the engine and combustor geometries. These four pieces of information consist of knowing the combustor entrance flow conditions, knowing the inlet entrance ρu, specifying the possible heat sink per kilogram of fuel, and having a knowledge of the value of A_V that should be assumed for the combustor being considered. Inlet and combustor entrance flow conditions are easily generated through the use of one of the many cycle programs that are generally available. In the course of conducting the combustor calculations used to produce the curve of figure 22, it was found to be possible to have an average value of A_V over the combustor of 2.0. To keep the average value of A_V of 2.0, the present investigation found that particular emphasis has to be placed on producing a combustor design which has a combustor area variation and fuel injection schedule through the combustor that is coordinated to produce essentially no positive pressure gradients. This type of combustor design results in keeping the boundary-layer distortion at a minimum and thus combustor cooling requirements as low as possible. Therefore, on the basis of the experience obtained during the present combustor heat-transfer calculations, a value of A_V of 2.0 is felt to be a reasonable assumption for use with the curve of figure 22 to produce reasonable estimates for combustor cooling requirements if the combustor is designed to have essentially no pressure gradients. In conclusion, the use of the correlation to predict combustor cooling should be limited to combustors with geometries somewhat similar to that of the Langley scramjet engine.

CONCLUDING REMARKS

In connection with research programs on hypersonic airbreathing propulsion, an integral method for predicting boundary-layer development in turbulent flow regions on two-dimensional or axisymmetric bodies has been developed through use of integral-momentum, moment of momentum, and energy equations together with appropriate auxiliary equations. The method has the capability of approximating nonequilibrium velocity distributions as well as the local surface friction in the presence of a pressure gradient. An approach is developed to the problem of predicting the heat transfer in a turbulent boundary layer in the presence of a high pressure gradient. No provision was included to account for a pressure gradient normal to the surface. The solution was derived with particular emphasis on its applicability to supersonic combustion; thus, real-gas flow effects were included. The real-gas capability of the integral boundary-layer equations used in the prediction method includes terms which account for the change in combustion products in a boundary layer but do not include terms which actually compute the chemical reactions in the boundary layer. The resulting integrodifferential boundary-layer method permits the estimation of the cooling requirements for scramjet engines.

Theoretical heat-transfer results are compared with experimental combustor and noncombustor heat-transfer data and show reasonable agreement. The theoretical heat-transfer method is used to predict heating and thus the cooling requirements for a sample engine sized by estimates of drags and at a range of altitudes for a vehicle between Mach numbers 6 and 10. These calculations indicate that in hypersonic engine design, certain design concepts should be incorporated to account for the resulting cooling requirements of the engine. The general design concepts imposed on hypersonic engine design by engine cooling restrictions indicate that when engine cooling is considered, scramjets are advantageous at Mach numbers of about 6.0 and above, that combustor pressures should be kept at the minimum required for efficient combustion, and that the positive pressure gradients in the combustor should be kept as small as possible. Also these engine cooling restrictions require that the combustor and nozzle wetted areas should be kept as small as possible; analysis of the sample engine indicates that the use of fuel injection struts provides a technique for reducing the ratio of combustor wetted area to its entrance area. The analysis of the sample engine also indicates that the operating Mach number range of an engine (relative to engine cooling requirements) can be increased if the fuel injection is designed to keep the combustion in the center of the combustor and away from the surface. The general design concepts imposed on hypersonic engine design by engine cooling restrictions were utilized in the design of the Langley scramjet engine module. The cooling requirements of the Langley scramjet engine module were found to be such that excess fuel heat sink is available over the

Mach number range considered. The nozzle design of the Langley scramjet engine module is very conservative and investigations are in progress which are aimed at reducing the nozzle length and wetted area by as much as 50 percent.

The present heat-transfer method is used to develop a combustor cooling requirement correlation for a combustor whose local flow properties throughout the combustor are computed one-dimensionally by assuming a linear area variation and a given heat release schedule. This correlation (calculations were made for Mach numbers 6, 8, and 10) can be used to obtain quick and reasonable estimates of cooling requirements for a combustor of this type without a long calculation procedure.

Langley Research Center,
National Aeronautics and Space Administration,
Hampton, Va., October 17, 1974.

APPENDIX

CORRELATION OF THE COMBUSTOR AND NOZZLE COOLING FOR A HYDROGEN FUELED SCRAMJET

The desired combustor cooling correlation results from the following relationship which is valid for a combustor's surface heat transfer:

$$\frac{Q_\Phi}{(\rho_\delta u_\delta)_{A_v}(h_{aw} - h_w)} \propto C_f R_A A_c \tag{30}$$

The parameter Q_Φ is the integrated total heat transfer. With the use of a simple compressibility type correction, as well as an approximate correction for the effect of a pressure gradient on the heat transfer, the following proportionality is obtained for the friction coefficient of equation (30)

$$C_f \propto \frac{1}{1 + \frac{\gamma - 1}{2} M_\infty^2} C_{f,i} \frac{A_v^2}{4} \tag{31}$$

The ratio of A_v^2 over 4 is an approximate correction on C_f to account for the pressure gradient effect on the heat transfer and is somewhat similar to that of equations (10) and (15). In the theoretical correlation, average values of A_v are used which are obtained by adding the values of A_v predicted at uniform intervals through the combustor and dividing by the number of A_v values. For a two-dimensional engine, the local incompressible frictional coefficient is given by

$$C_{f,i} \propto \frac{1}{\left(q_\infty A_I^{1/2}\right)^{1/7}} \tag{32}$$

It is also assumed that

$$h_{aw} \propto h_{t,\infty} \tag{33}$$

and

$$(\rho_\delta u_\delta)_{A_v} \propto (\rho_\delta u_\delta)_3 \, f\left(\frac{A_4}{A_3}\right) \tag{34}$$

The proportionality presented in equation (34) is a result of attempting to account for the effect of area change across the combustor or nozzle on the local mass flow per unit area. The flow area distribution through the combustor is assumed to be approximated by the linear relation with x as given by

$$A_L = A_3 + \frac{x}{L}\left(A_4 - A_3\right) \tag{35}$$

where L is the total combustor length. The distribution of the mass flow per unit area through the combustor is given by

$$\left(\rho_\delta u_\delta\right)_L = \left(\rho_\delta u_\delta\right)_3 \frac{A_3}{A_3 + \frac{x}{L}\left(A_4 - A_3\right)} \tag{36}$$

The average mass flow per unit area weighted by combustor surface area is given by

$$\left(\rho_\delta u_\delta\right)_{A_v} \propto \frac{2\int_0^L \left(\rho_\delta u_\delta\right)_3 A_3 \left[\frac{W_L + H_L}{A_3 + \frac{x}{L}\left(A_4 - A_3\right)}\right] dx}{A_c} \tag{37}$$

where W_L and H_L is the local width and height of the combustor and is assumed to be given by

$$W_L = H_L = \left(A_L\right)^{1/2} \tag{38}$$

The combustor wetted area is given by

$$A_c = 2\left(A_4^{1/2} + A_3^{1/2}\right)L \tag{39}$$

Substitution of equations (38) and (39) into equation (37) gives upon integration and rearranging

$$\left(\rho_\delta u_\delta\right)_{A_v} \propto \frac{4\left(\rho_\delta u_\delta\right)_3}{\frac{A_4}{A_3}} \frac{1 - 2\left(\frac{A_3}{A_4}\right)^{1/2} + \frac{A_3}{A_4}}{1 - 2\frac{A_3}{A_4} + \left(\frac{A_3}{A_4}\right)^2} \tag{40}$$

and thus,

$$f\left(\frac{A_4}{A_3}\right) = \frac{4}{\frac{A_4}{A_3}} \frac{1 - 2\left(\frac{A_3}{A_4}\right)^{1/2} + \frac{A_3}{A_4}}{1 - 2\frac{A_3}{A_4} + \left(\frac{A_3}{A_4}\right)^2} \tag{41}$$

The total fuel heat sink can be expressed by

$$Q_f = (\rho u A)_I J \tag{42}$$

Substitution of equations (31) to (34) into equation (30) gives after rearranging

$$\frac{Q_\Phi}{Q_f} \frac{(\rho u)_I \left(q_\infty A_I^{1/2}\right)^{1/7} \left(1 + \frac{\gamma - 1}{2} M_\infty^2\right) \frac{4}{A_V^2} J}{\left[\rho_\delta u_\delta (h_{t,\delta} - h_w)\right]_3} \propto \frac{R_A A_c}{A_I} f\left(\frac{A_4}{A_3}\right) \tag{43}$$

The relationship between the total heat transfer $Q_{\Phi=1.0}$ to a combustor for fuel equivalence ratio of 1.0 and the total heat transfer to a combustor for fuel equivalence ratios less than 1.0 but greater than zero is assumed to be given by

$$Q_{\Phi=1.0} \propto \frac{Q_\Phi}{\Phi} \tag{44}$$

Substituting equation (44) into equation (43) and assuming that the Reynolds analogy factor is constant gives after rearranging

$$\frac{Q_\Phi}{Q_f} \frac{(\rho u)_I \left(q_\infty A_I^{1/2}\right)^{1/7} \left(1 + \frac{\gamma - 1}{2} M_\infty^2\right) \frac{4}{A_V^2} J}{\left[\rho_\delta u_\delta (h_{t,\delta} - h_w)\right]_3} \propto \frac{\Phi A_c}{A_I} f\left(\frac{A_4}{A_3}\right) \tag{45}$$

REFERENCES

1. Ferri, A.: Review of SCRAMJET Propulsion Technology. J. Aircraft, vol. 5, no. 1, Jan.-Feb. 1968, pp. 3-10.

2. Weber, Richard J.; and MacKay, John S.: An Analysis of Ramjet Engines Using Supersonic Combustion. NACA TN 4386, 1958.

3. Carlson, C. H.; and Brewster, R. E.: Applications Studies for the Dual Mode, Fixed Geometry, Hydrogen Fueled Scramjet. Vol. I: Parametric Performance and Design of a Baseline Engine. AFAPL-TR-67-130, Vol. I, U.S. Air Force, Sept. 1967. (Available from DDC as AD 388 533.)

4. Pagel, L. L.; and Warmbold, W. R.: Active Cooling of a Hydrogen Fueled Scramjet Engine. AIAA Paper No. 68-1091, Oct. 1968.

5. Lee, Dorothy B.; and Faget, Maxime A.: Charts Adapted From Van Driest's Turbulent Flat-Plate Theory for Determining Values of Turbulent Aerodynamic Friction and Heat-Transfer Coefficients. NACA TN 3811, 1956.

6. Eckert, Ernst R. G.: Survey on Heat Transfer at High Speeds. WADC Tech. Rep. 54-70, U.S. Air Force, Apr. 1954.

7. Neal, Luther, Jr.; and Bertram, Mitchel H.: Turbulent-Skin-Friction and Heat-Transfer Charts Adapted From the Spalding and Chi Method. NASA TN D-3969, 1967.

8. Levin, Victor; and Fabish, Thomas J.: Thermal Effects of Shockwave Turbulent Boundary Layer Interaction at Mach Numbers 3 and 5. NA 62 H-795 (Contract NO_W 61-0679-C), North Am. Aviation, Inc., Nov. 12, 1962.

9. Johnson, Charles B.; and Kaufman, Louis G., II: Interference Heating From Interactions of Shock Waves With Turbulent Boundary Layers at Mach 6. NASA TN D-7649, 1974.

10. Billig, Frederick S.; and Grenleski, S. E.: Heat Transfer in Supersonic Combustion Processes. Paper presented at Fourth International Heat Transfer Conference (Versailles, France), Aug. 1970.

11. Alber, Irwin E.; and Coats, Douglas E.: Analytical Investigations of Equilibrium and Nonequilibrium Compressible Turbulent Boundary Layers. AIAA Paper No. 69-689, June 1969.

12. Rubesin, Morris W.: A Modified Reynolds Analogy for the Compressible Turbulent Boundary Layer on a Flat Plate. NACA TN 2917, 1953.

13. Nestler, D. E.; and Goetz, R.: Survey of Theoretical and Experimental Determinations of Skin Friction in Compressible Boundary Layers: Part II. The Turbulent Boundary on a Flat Plate. Tech. Inform. Ser. No. R58SD270 (Contract AF 04(645)-24), Missile Ord. Syst. Dep., Gen. Elec. Co., Jan. 29, 1959.

14. Pinckney, S. Z.: Method for Predicting Compressible Turbulent Boundary Layers in Adverse Pressure Gradients. NASA TM X-2302, 1971.

15. Maslowe, S. A.; and Benson, J. L.: Computer Program for the Design and Analysis of Hypersonic Inlets. Rep. No. 18079 (Contract NAS 2-1460), Lockheed-California Co., Aug. 10, 1964. (Available as NASA CR-77749.)

16. Reshotko, Eli; and Tucker, Maurice: Approximate Calculation of the Compressible Turbulent Boundary Layer With Heat Transfer and Arbitrary Pressure Gradient. NACA TN 4154, 1957.

17. Stroud, John F.; and Miller, Leonard D.: An Experimental and Analytical Investigation of Hypersonic Inlet Boundary Layers. Volumes I and II. AFFDL-TR-65-123, Vols. I and II, U.S. Air Force, Aug. 1965. (Available from DDC as AD 621 343 and AD 621 344.)

18. Herring, H. James; and Mellor, George L.: A Method of Calculating Compressible Turbulent Boundary Layers. NASA CR-1144, 1968.

19. Harris, Julius E.: Numerical Solution of the Equations for Compressible Laminar, Transitional, and Turbulent Boundary Layers and Comparisons With Experimental Data. NASA TR R-368, 1971.

20. Hixon, Barbara A.; Beckwith, Ivan E.; and Bushnell, Dennis M.: Computer Program for Compressible Laminar or Turbulent Nonsimilar Boundary Layers. NASA TM X-2140, 1971.

21. Economos, Constantino; and Boccio, John: An Investigation of the High Speed Turbulent Boundary Layer With Heat Transfer and Arbitrary Pressure Gradient. Part I – Summary Report. NASA CR-1679, 1970.

22. Kuhn, Gary D.: Calculation of Compressible, Nonadiabatic Boundary Layers in Laminar, Transitional and Turbulent Flow by the Method of Integral Relations. NASA CR-1797, 1970.

23. Mellor, G. L.; and Gibson, D. M.: Equilibrium Turbulent Boundary Layers. J. Fluid Mech., vol. 24, pt. 2, Feb. 1966, pp. 225-253.

24. Pinckney, S. Z.: Static-Temperature Distribution in a Flat-Plate Compressible Turbulent Boundary Layer With Heat Transfer. NASA TN D-4611, 1968.

25. Hoydysh, Walter G.; and Zakkay, Victor: An Experimental Investigation of Hypersonic Turbulent Boundary Layers in Adverse Pressure Gradient. AIAA J., vol. 7, no. 1, Jan. 1969, pp. 105-116.

26. Maise, George; and McDonald, Henry: Mixing Length and Kinematic Eddy Viscosity in a Compressible Boundary Layer. AIAA J., vol. 6, no. 1, Jan. 1968, pp. 73-80.

27. Coles, Donald: The Law of the Wake in the Turbulent Boundary Layer. J. Fluid Mech., vol. 1, pt. 2, July 1956, pp. 191-226.

28. Deissler, R. G.; and Loeffler, A. L., Jr.: Analysis of Turbulent Flow and Heat Transfer on a Flat Plate at High Mach Numbers With Variable Fluid Properties. NASA TR R-17, 1959. (Supersedes NACA TN 4262.)

29. Bradshaw, P.: The Response of a Constant-Pressure Turbulent Boundary Layer to the Sudden Application of an Adverse Pressure Gradient. NPL Aero Report 1219, Brit. A.R.C., Jan. 6, 1967.

30. Kaye, G. W. C.; and Laby, T. H.: Tables of Physical and Chemical Constants and Some Mathematical Functions. Thirteenth ed., John Wiley & Sons, Inc., 1966.

31. Moeckel, W. E.; and Weston, Kenneth C.: Composition and Thermodynamic Properties of Air in Chemical Equilibrium. NACA TN 4265, 1958.

32. Lynes, Larry L.; Nielsen, Jack N.; and Kuhn, Gary D.: Calculation of Compressible Turbulent Boundary Layers With Pressure Gradients and Heat Transfer. NASA CR-1303, 1969.

33. McClinton, Charles R.: The Effect of Injection Angle on the Interaction Between Sonic Secondary Jets and a Supersonic Free Stream. NASA TN D-6669, 1972.

34. Henry, John R.; and Anderson, Griffin Y.: Design Considerations for the Airframe-Integrated Scramjet. NASA TM X-2895, 1973.

35. Becker, John V.: New Approaches to Hypersonic Aircraft. Paper presented at Seventh Congress of International Council of the Aeronautical Sciences (Rome, Italy), Sept. 1970.

36. Becker, John V.: Prospects for Actively Cooled Hypersonic Transports. Astronaut. & Aeronaut., vol. 9, no. 8, Aug. 1971, pp. 32-39.

37. Henry, John R.; and Beach, H. Lee: Hypersonic Air-Breathing Propulsion Systems. Vehicle Technology for Civil Aviation – The Seventies and Beyond, NASA SP-292, 1971, pp. 157-177.

TABLE I.- COMBUSTOR COOLING CASES

Symbol	M_∞	q_∞, N/m^2	Fuel, Φ	A_I, m^2	A_4/A_3	M_I	$h_{t,\infty}$, MJ/kg	T_w, K	h_w, MJ/kg	H_2 heat sink, MJ/kg	$(\rho u)_I$, $(kg/m^2)/sec$	$(\rho u)_3$, $(kg/m^2)/sec$	Altitude, m	A_c, m^2	Fuel injection type
○	6	1.68×10^4	1.0	3.642	2.5	4.6	2.0315	1256	1.3420	14.29	40.95	222.44	3.42×10^4	11.854	Normal
□	6		1.0											17.001	
◇	6		.75											11.854	
△	6		.75											17.001	
◸	6		.5		↓									11.854	
▱	6				2.0									↓	
⌓	6														
◇	6			↓	↓	↓	↓				↓	↓	↓	5.927	
◇	8		.75	7.809	2.5	5.7	3.2578				40.82	264.22	3.75×10^4	28.707	
⌓	8			7.809	1.4	5.7	3.2578				40.82	264.22	3.75×10^4	28.707	
○	10			7.432	2.5	6.56	5.3288				36.7	253.70	4.08×10^4	25.966	
□	10			↓	1.4	↓	↓				↓	↓	↓	↓	
◇	10				1.4										
△	10				1.0										
◸	10				1.4										
⌓	10				1.4										
◇	10				1.0									12.979	
◇	10				1.4									↓	
△	10			↓	1.4	↓	↓	↓	↓	↓	↓	↓	↓	↓	
○	10	4.78×10^4	1.0	5.87	5.04	7.31	4.9254	1111	1.1745		89.7	893.29	3.38×10^4	29.856	
□	10			5.87	3.526	↓	↓	↓	↓		↓	↓	↓	26.408	
◇	10			4.19	5.04									26.622	
△	10			↓	5.04									53.245	
◸	10				3.526	↓	↓				↓	↓	↓	47.957	
●	6				5.04	4.92	1.8355				109.1	946.33	2.68×10^4	26.622	Parallel
■	6				↓	4.92	1.8355				109.1	946.33	2.68×10^4	61.519	
◆	8			↓		6.21	3.1447				97.4	951.86	3.08×10^4	26.622	
▲	10			5.87		7.31	4.9254				89.7	893.29	3.38×10^4	29.856	
◣	10			4.19		↓	↓				↓	↓	↓	26.622	
◗	10			↓										26.622	
◗	8			↓	↓	6.21	3.1447	↓	↓	↓	97.4	951.86	3.08×10^4	61.519	↓

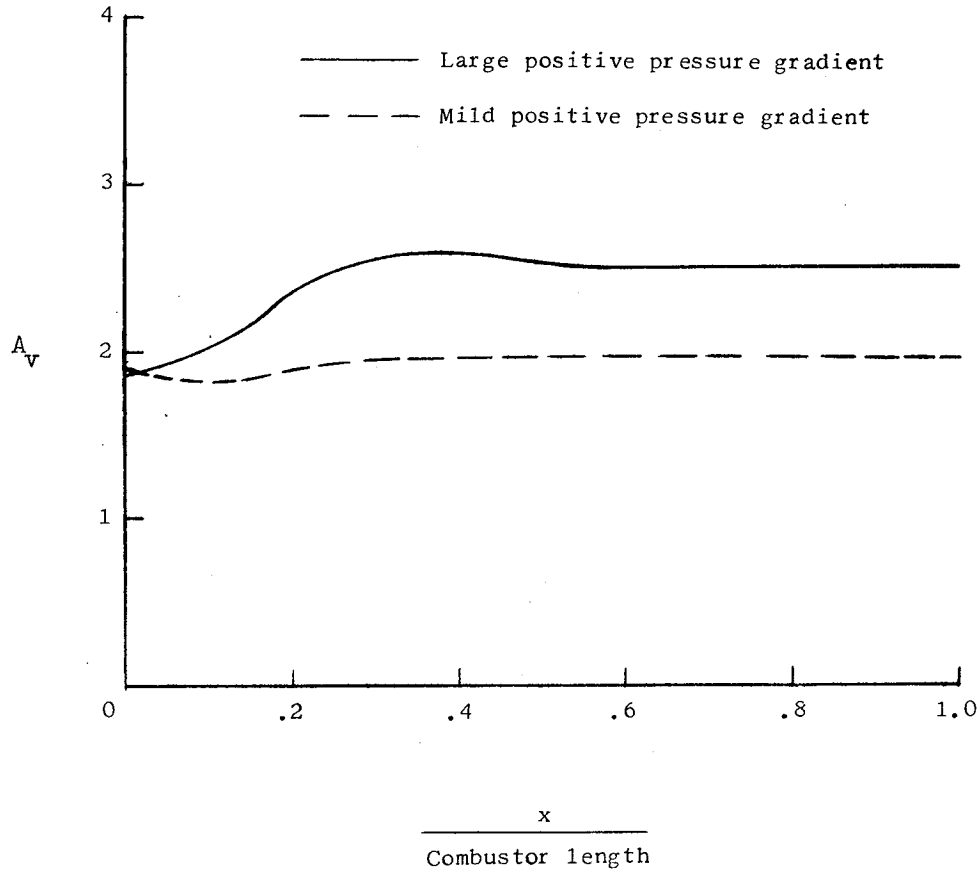

Figure 1.- Distribution of velocity profile parameter A_V in a combustor at $M_\infty = 10$.

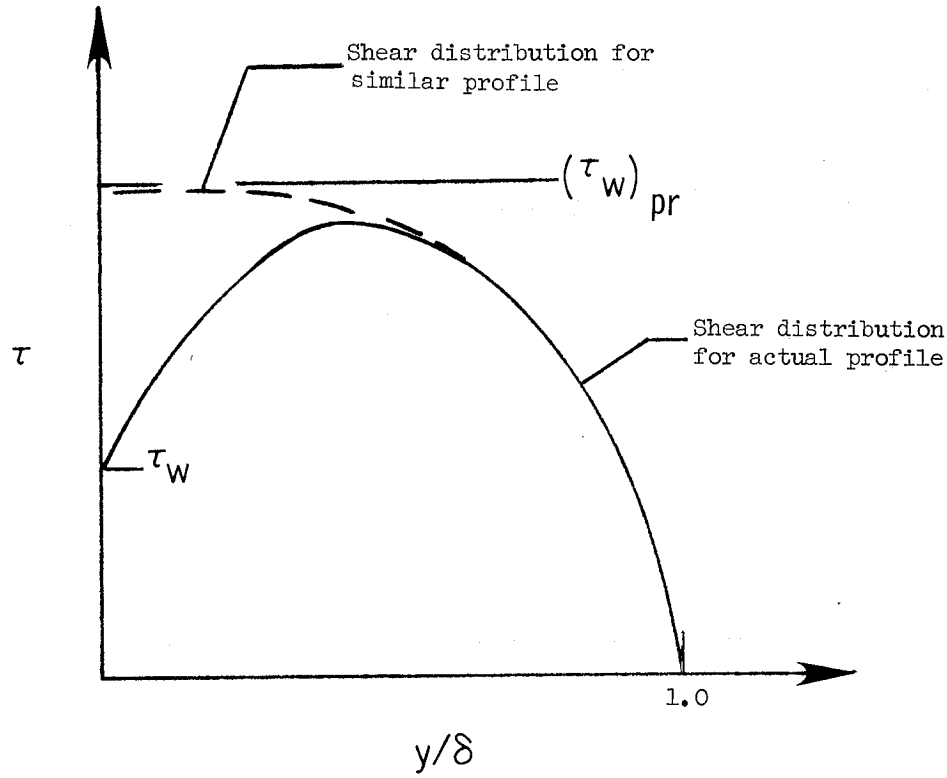

Figure 2.- Boundary-layer shear distributions.

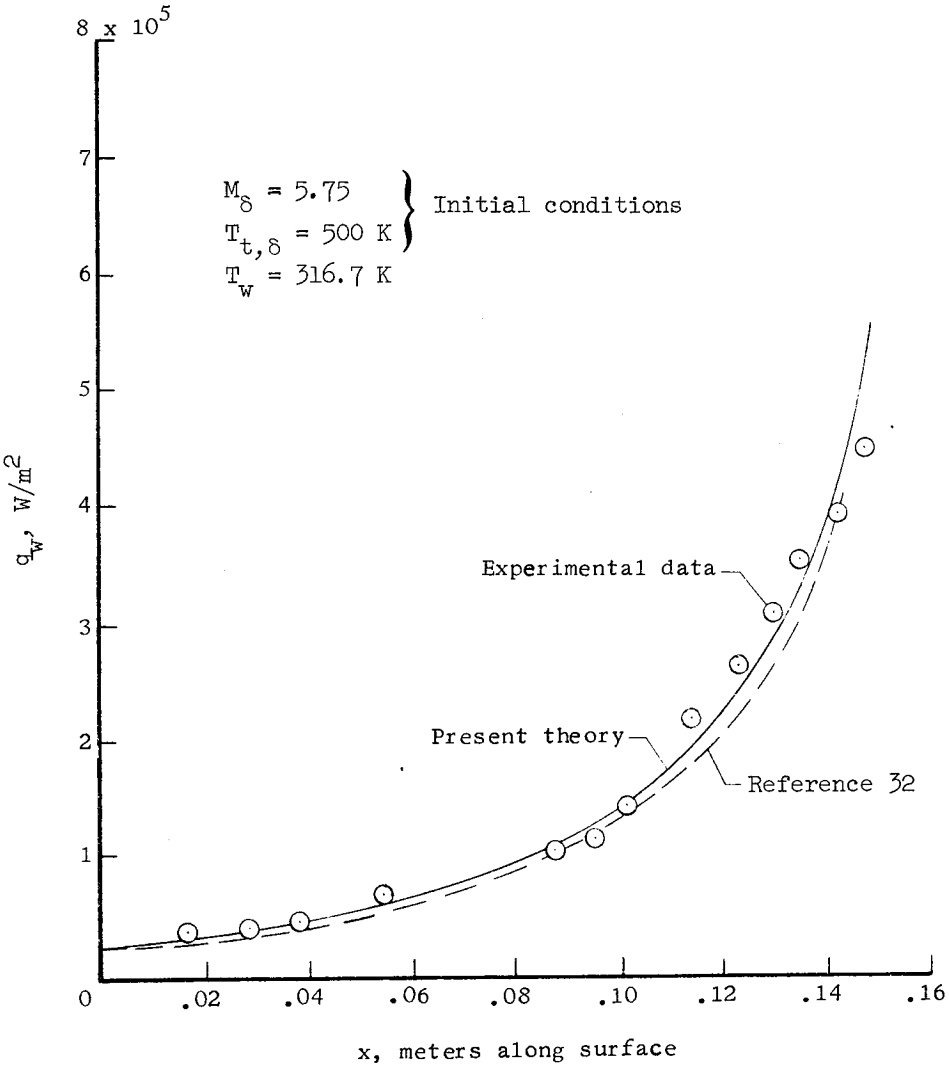

Figure 3.- Surface heat transfer on a 42° turning angle polynomial flare of reference 25.

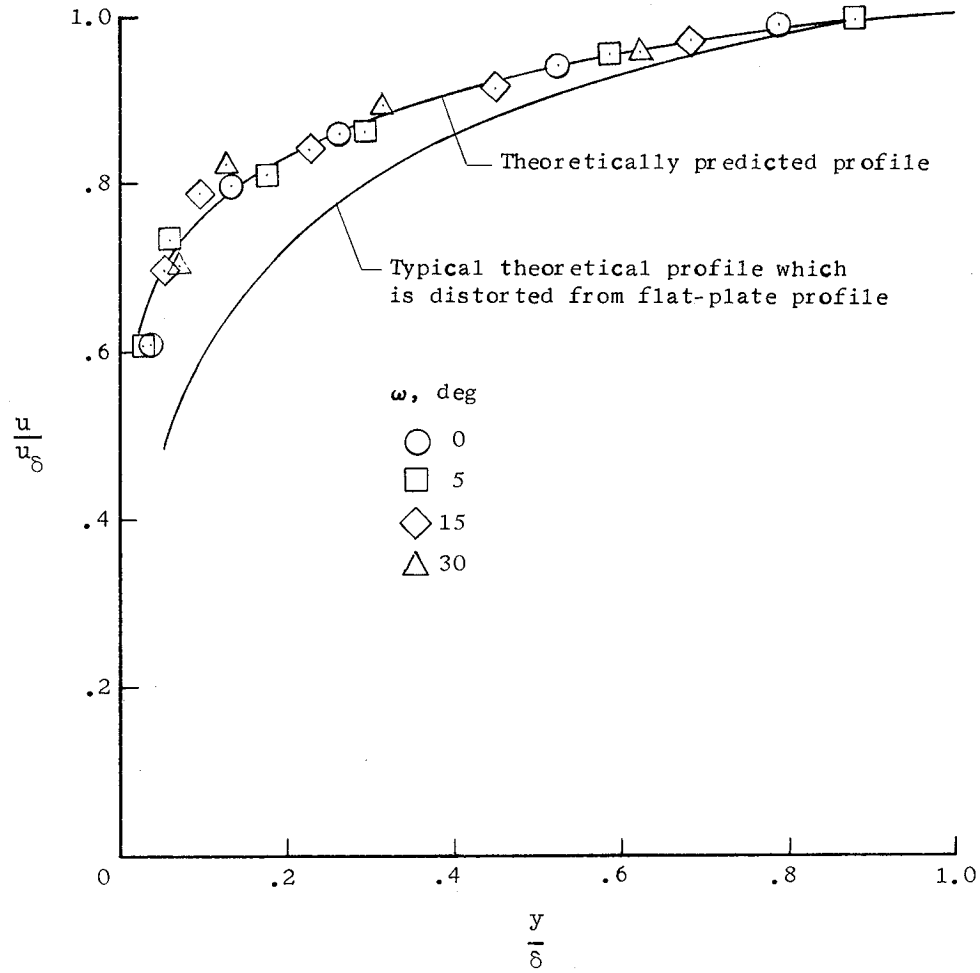

Figure 4.- Velocity profiles on a 42° turning angle polynomial flare of reference 25.

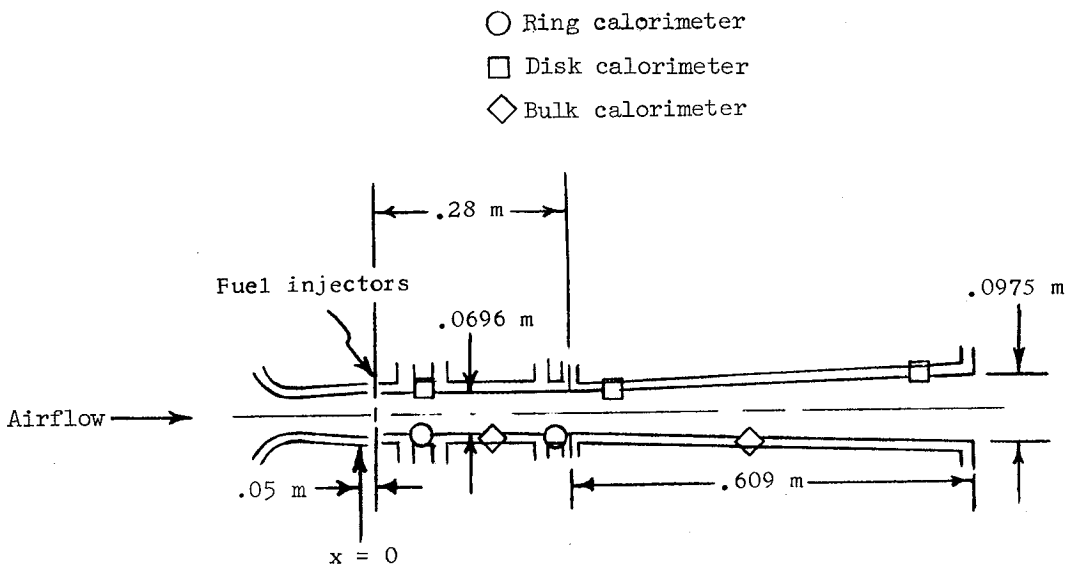

Figure 5.- Combustor configuration of reference 10.

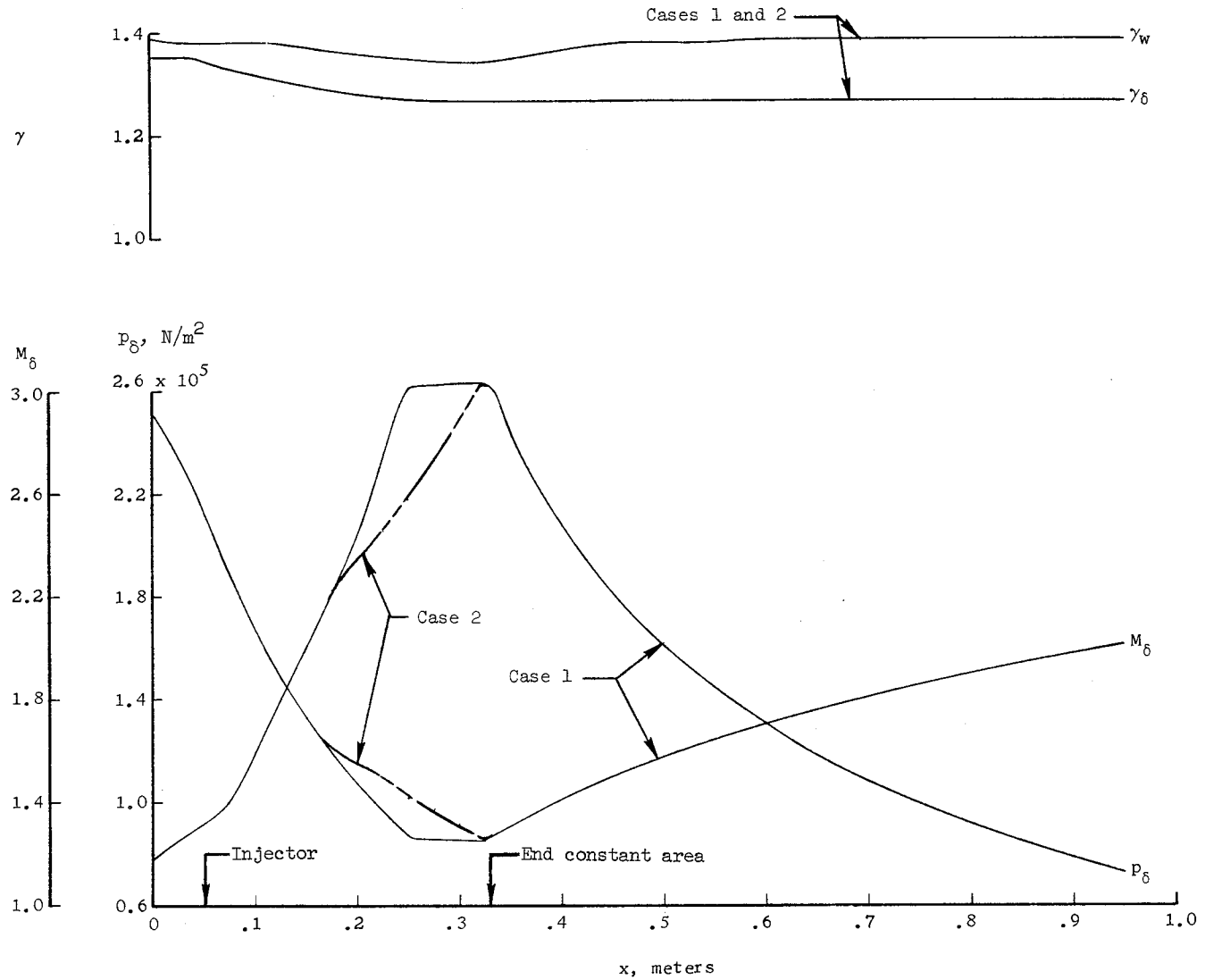

(a) γ_δ, γ_w, p_δ, and M_δ.

Figure 6.- Boundary-layer edge flow parameters for cases 1 and 2.

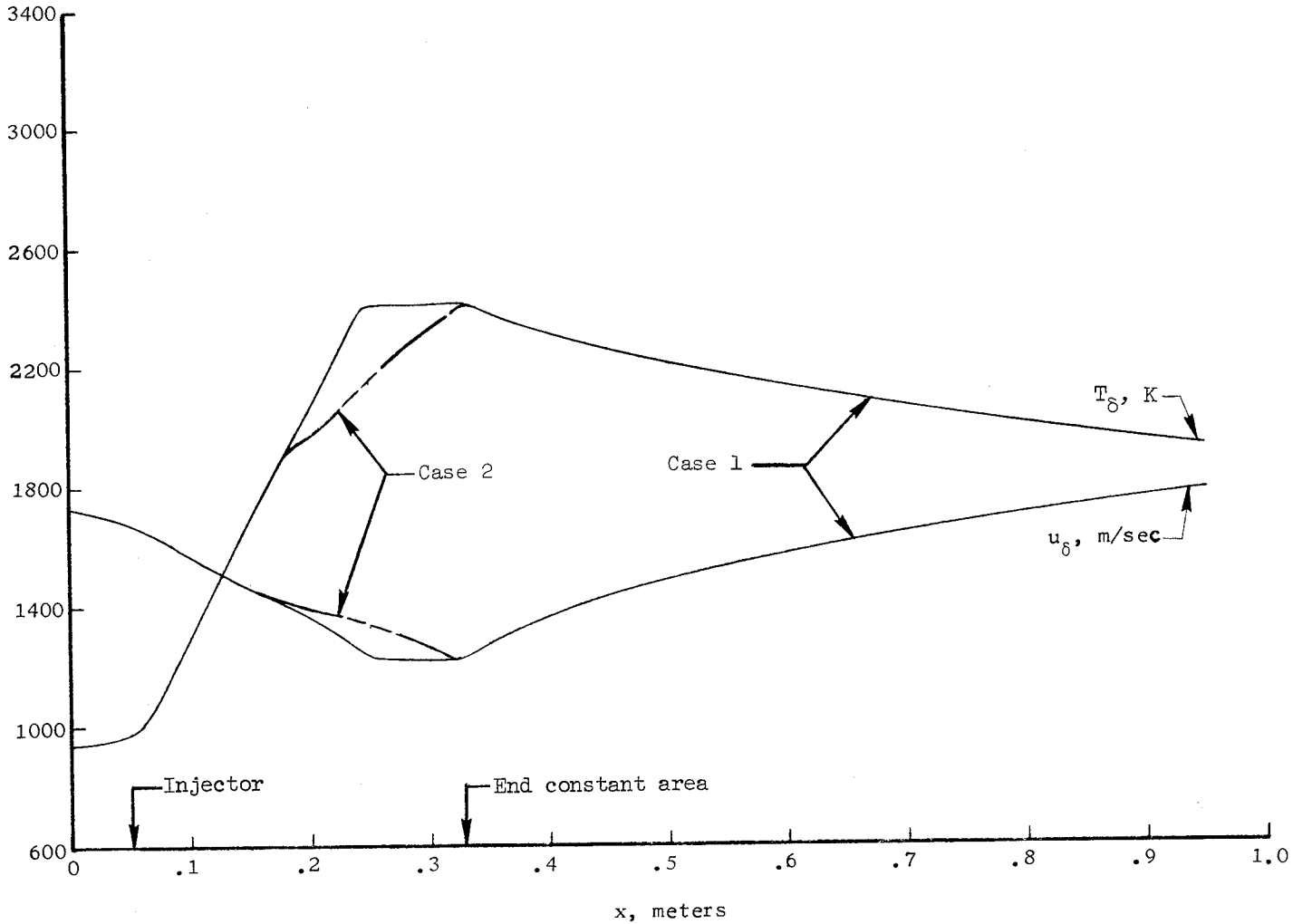

(b) T_δ and u_δ.

Figure 6.- Continued.

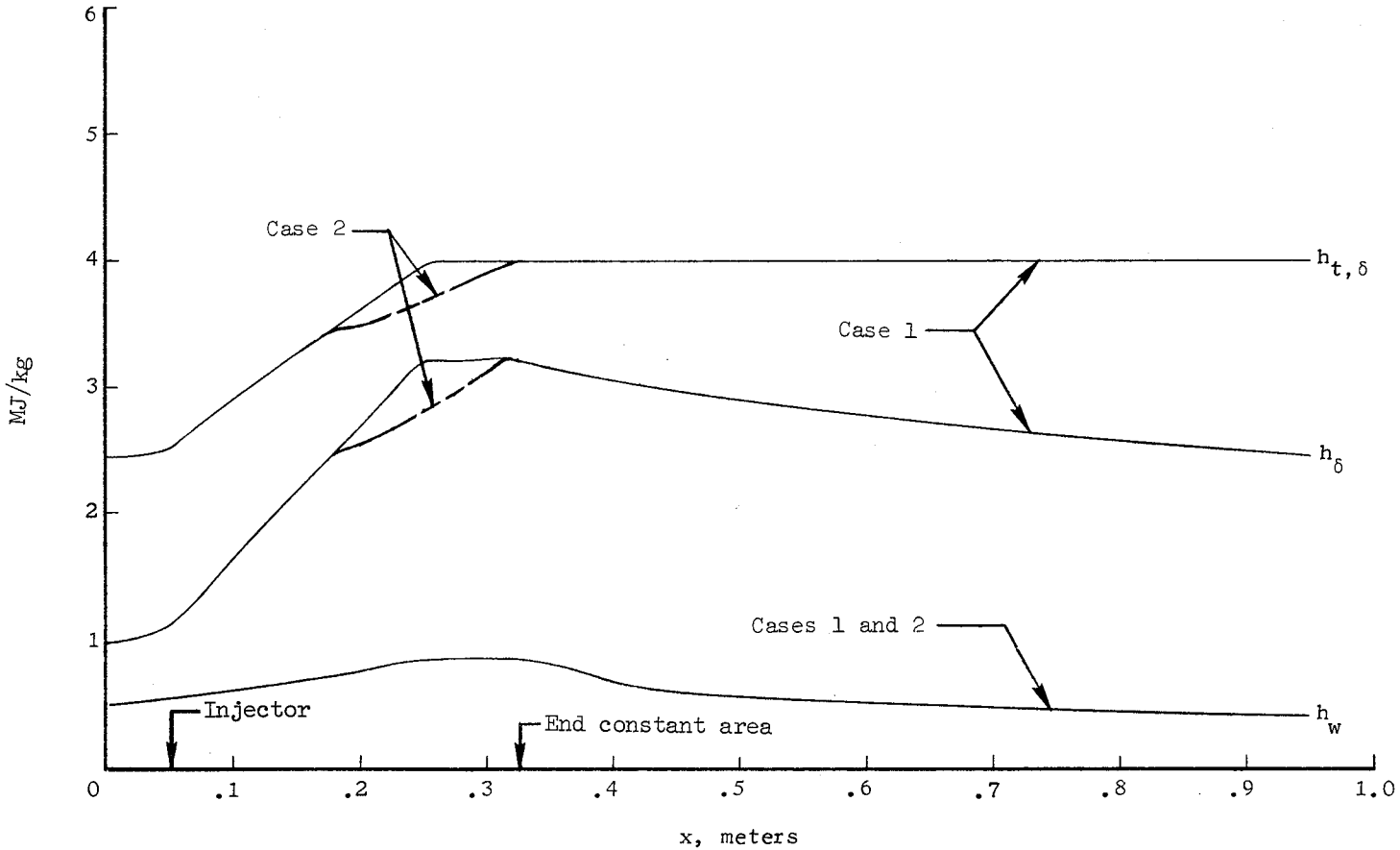

(c) h_w, h_δ, and $h_{t,\delta}$.

Figure 6.- Concluded.

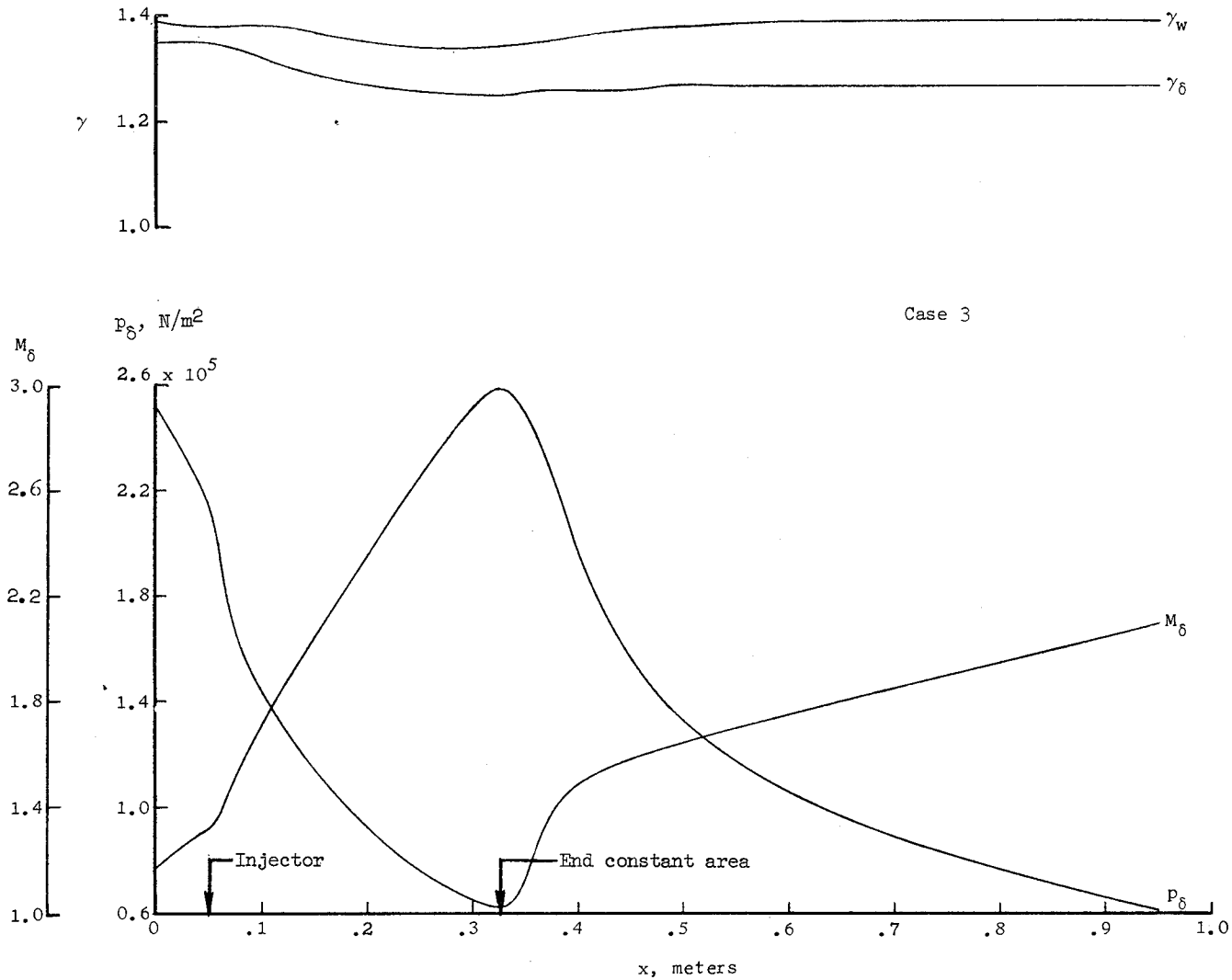

(a) γ_δ, γ_w, p_δ, and M_δ.

Figure 7.- Boundary-layer edge flow parameters for case 3.

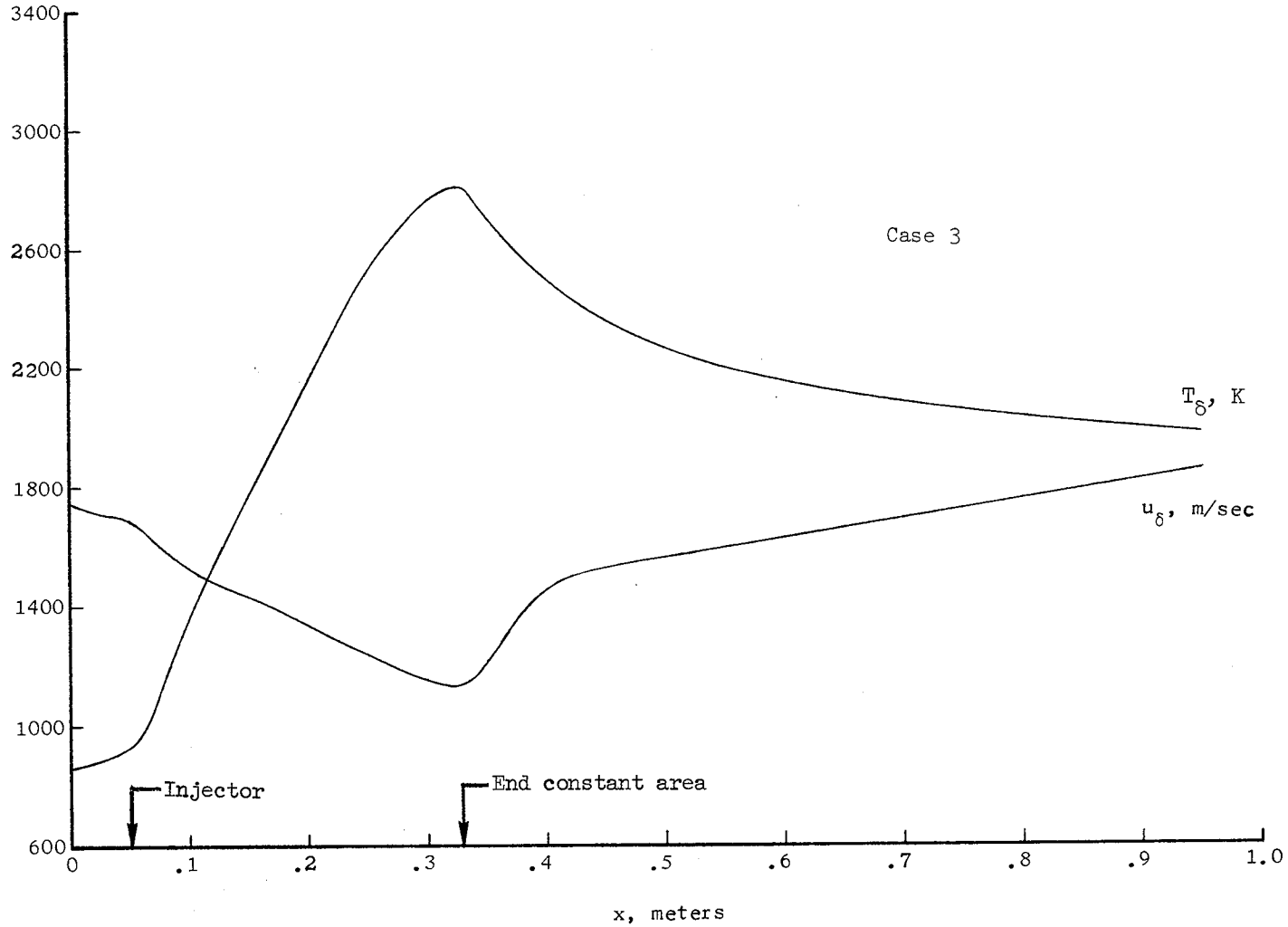

(b) T_δ and u_δ.

Figure 7.- Continued.

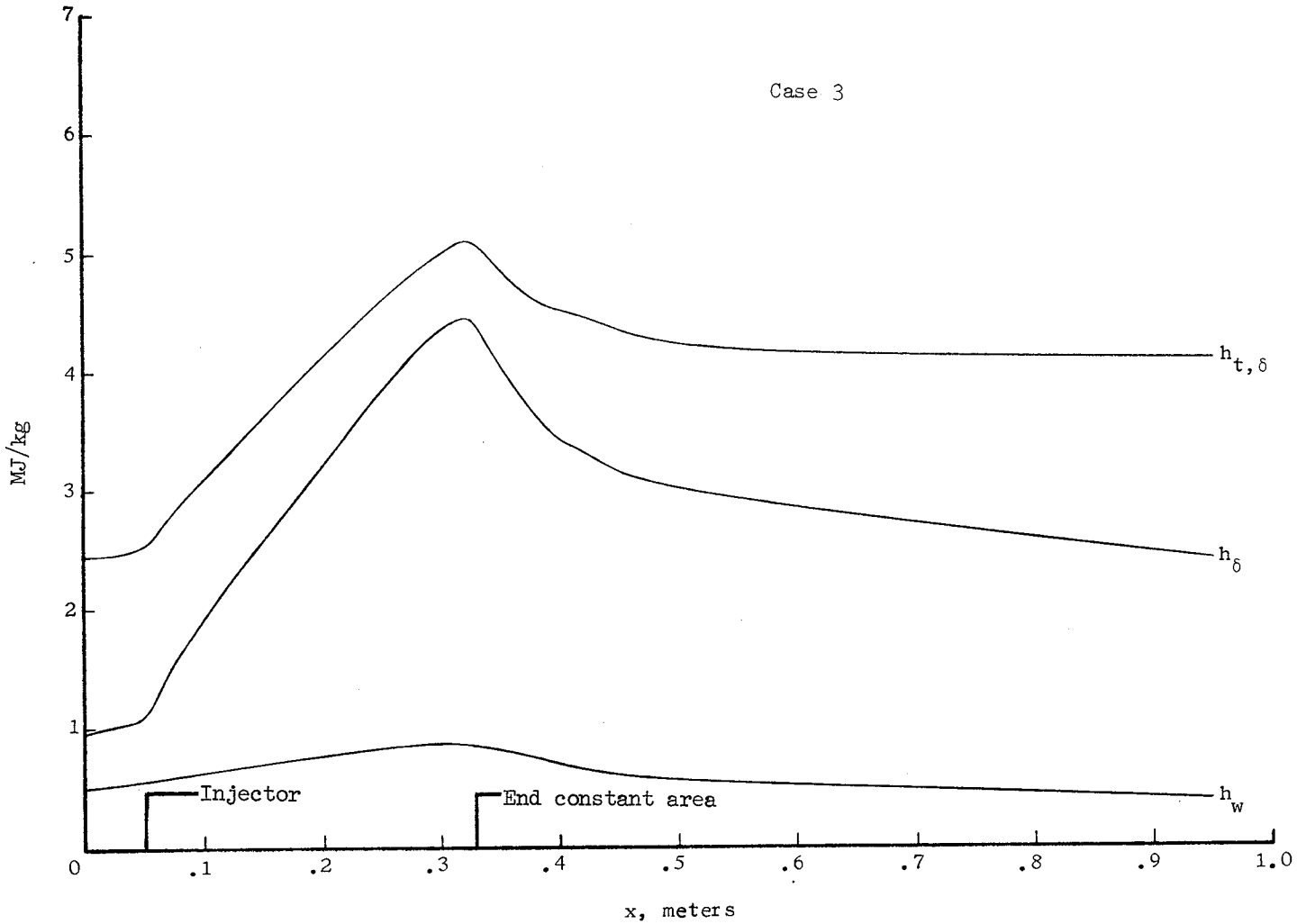

(c) h_w, h_δ, and $h_{t,\delta}$.

Figure 7.- Concluded.

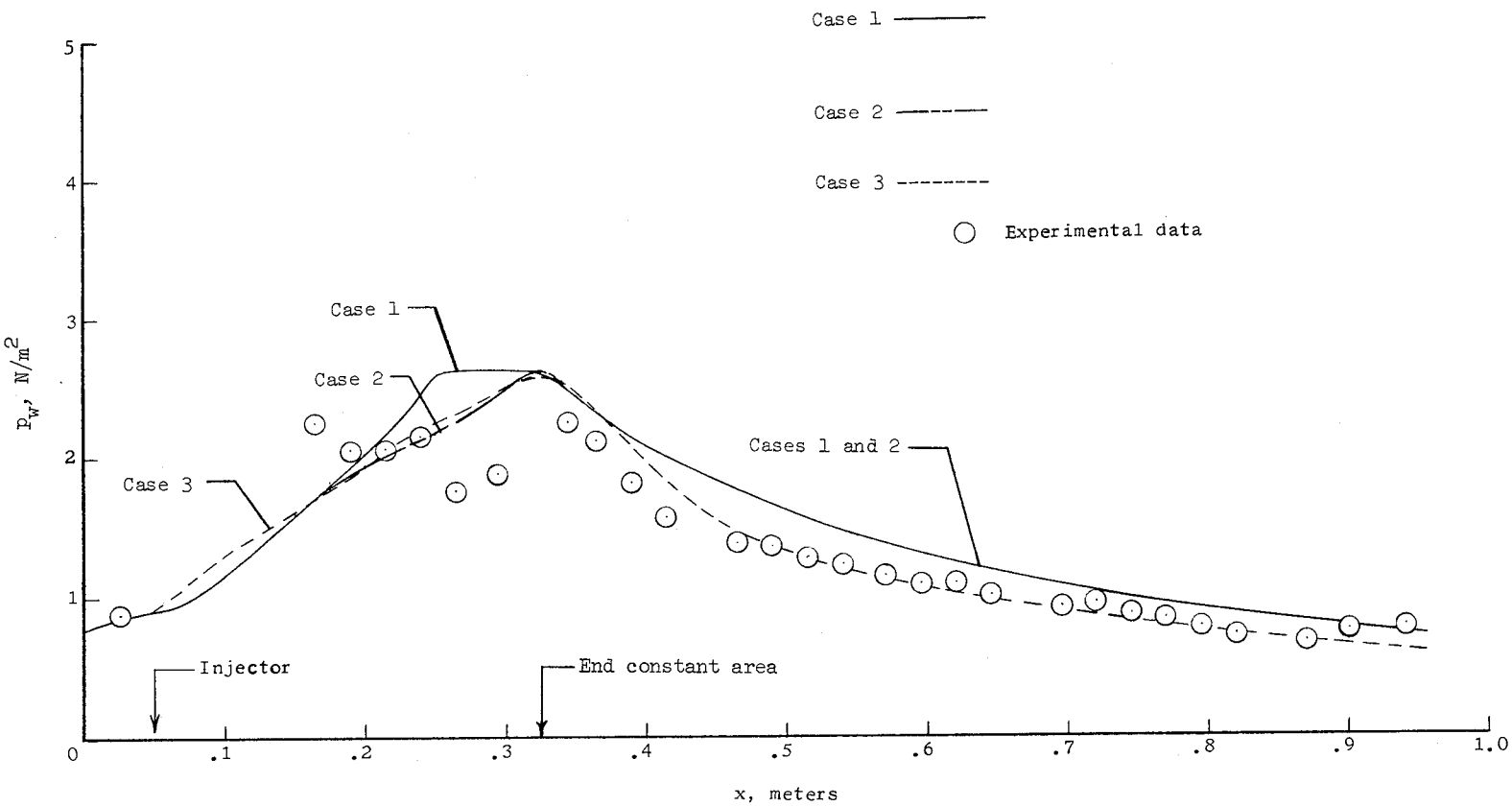

Figure 8.- Experimental static-pressure distribution through the combustor of reference 10 as compared with the theoretical static-pressure distributions of cases 1, 2, and 3.

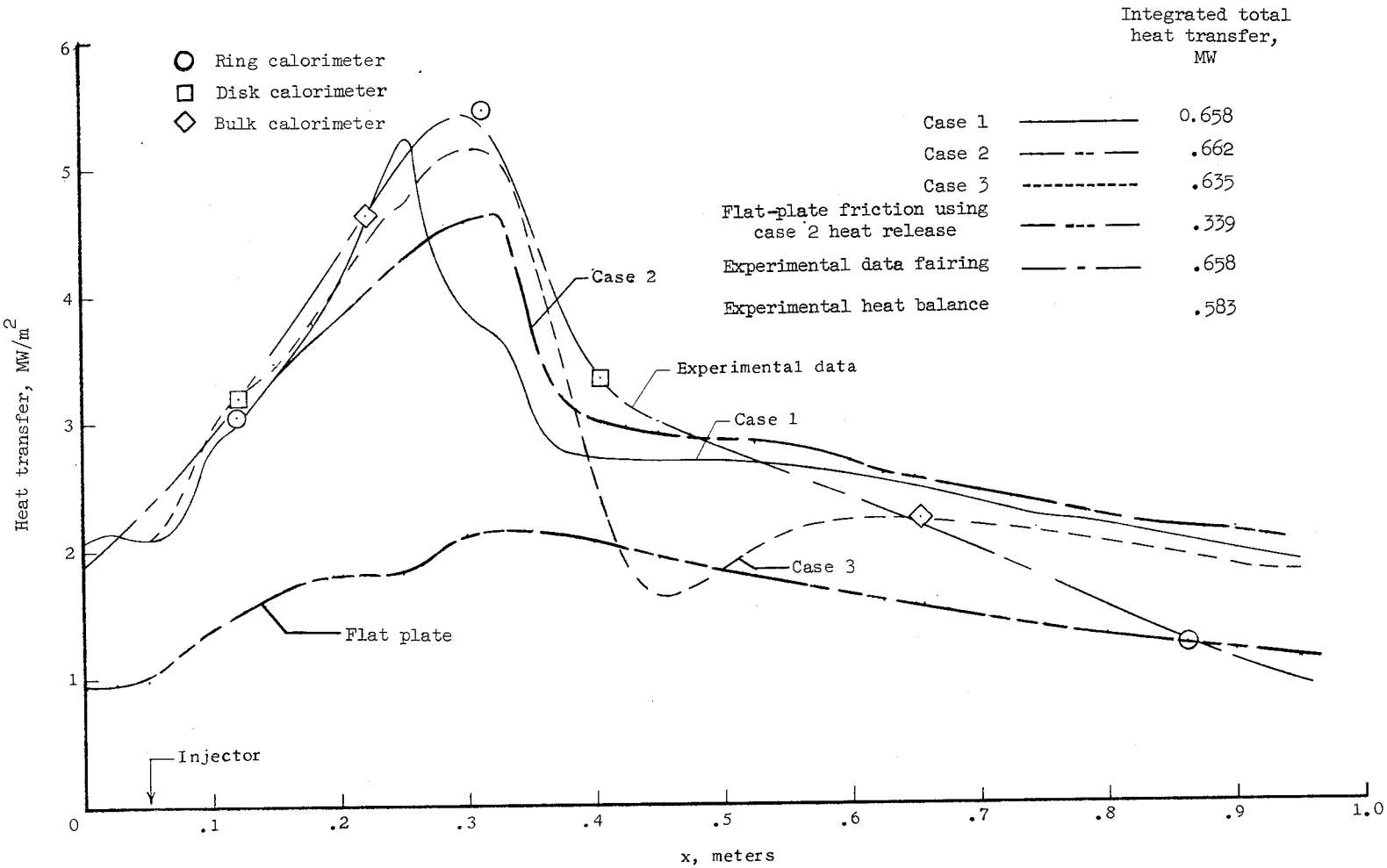

Figure 9.- Experimental surface heat-transfer distribution through the combustor of reference 10 as compared with the theoretically predicted distributions of cases 1, 2, and 3.

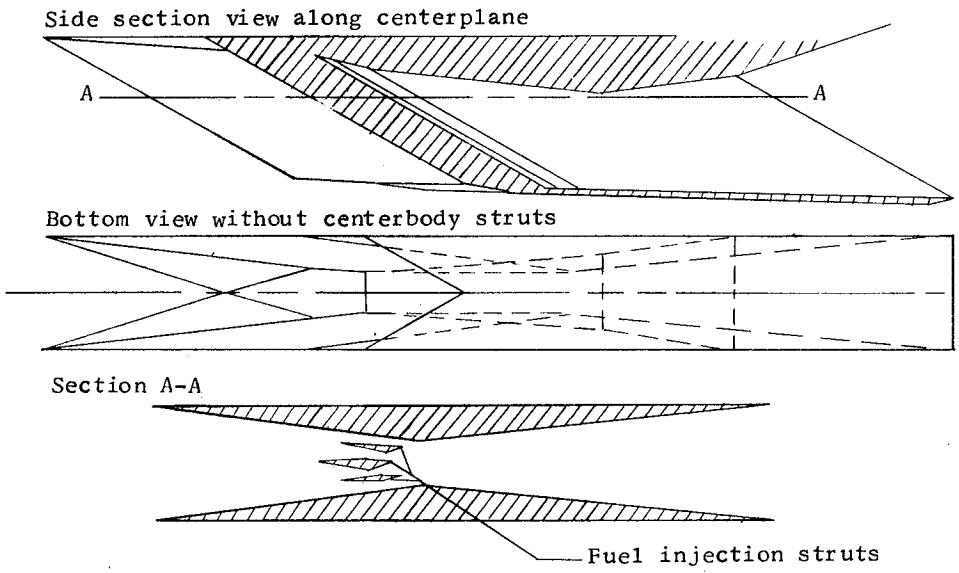

Figure 10.- Langley scramjet module.

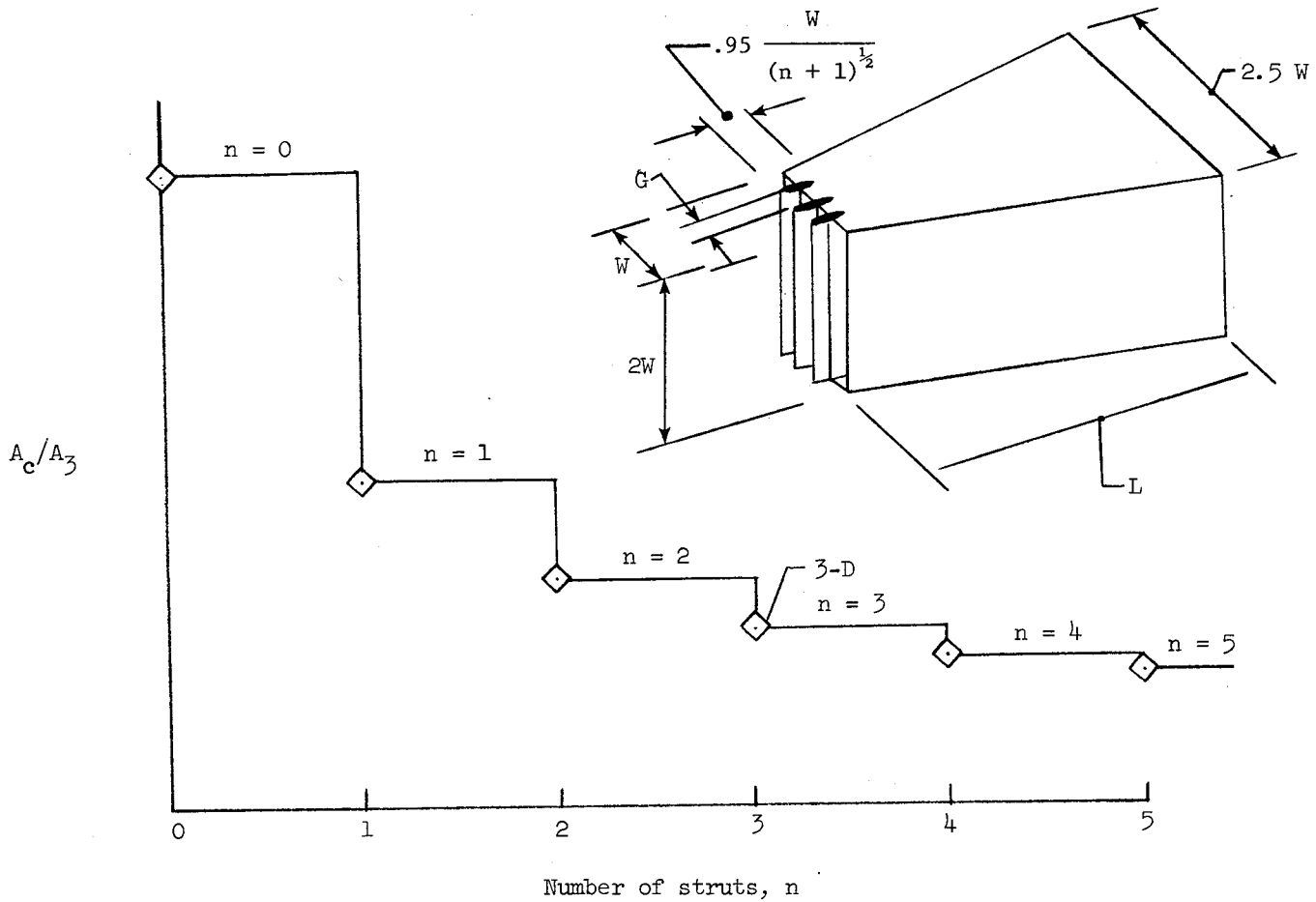

Figure 11.- The effect of fuel injection struts on combustor wetted area.

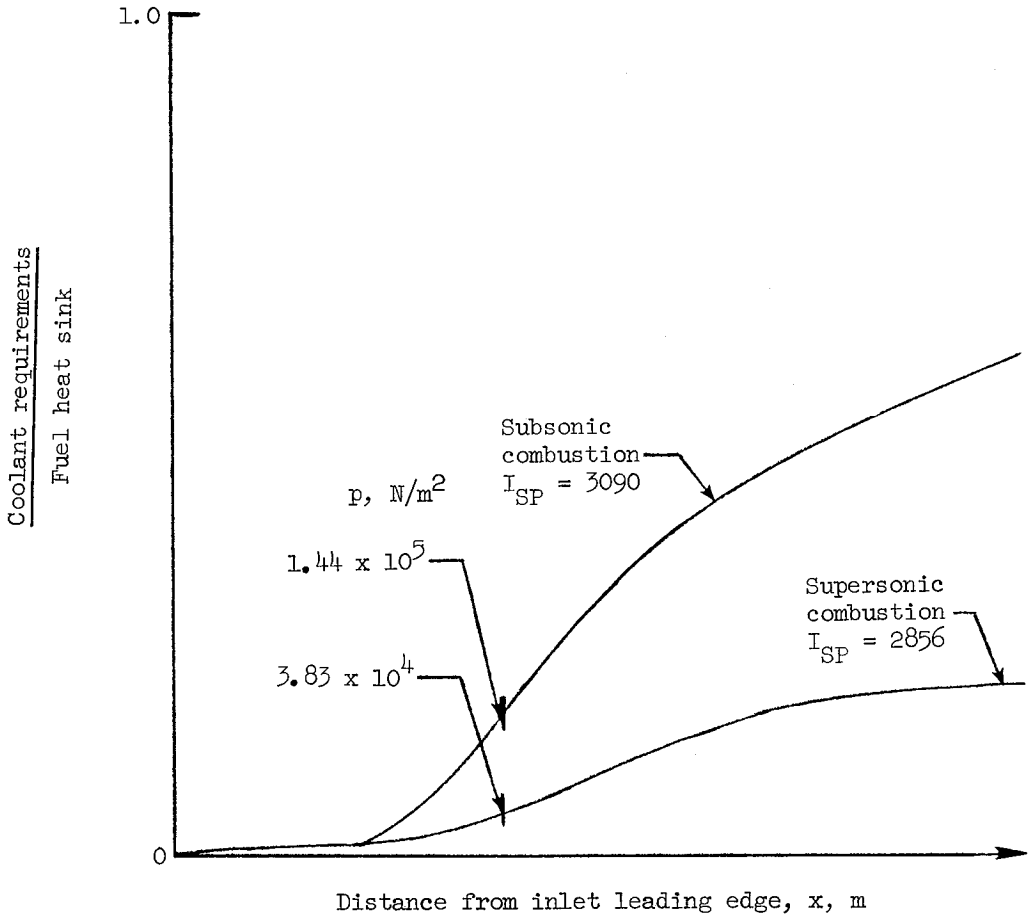

Figure 12.- Effect of combustion mode on cooling. $M_\infty = 6.0$; $\Phi = 1.0$; altitude, 34 200 meters.

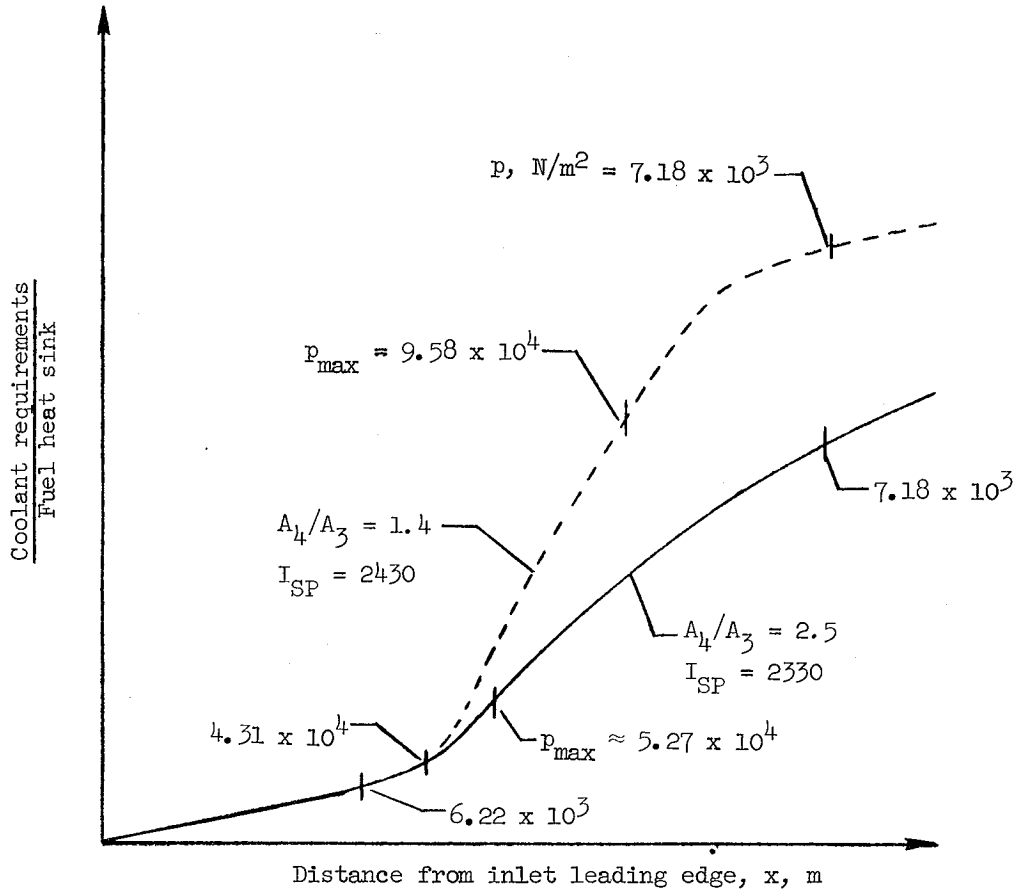

Figure 13.- Effect of combustor area ratio on cooling. M_∞ = 8; Φ = 0.75; altitude, 37 500 meters.

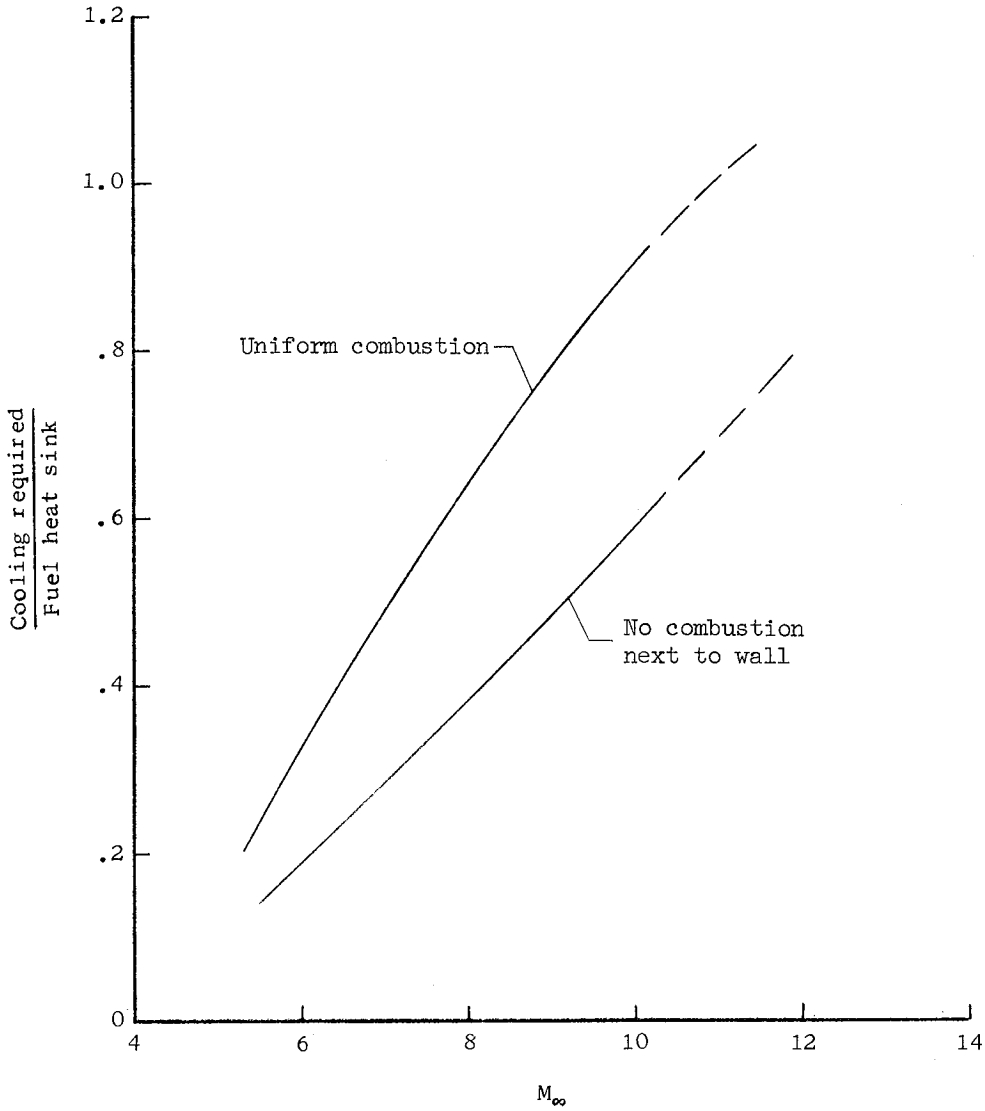

Figure 14.- Effect of protecting combustor wall from combustion enthalpies. $A_4/A_3 = 2.5$; $\Phi = 0.75$.

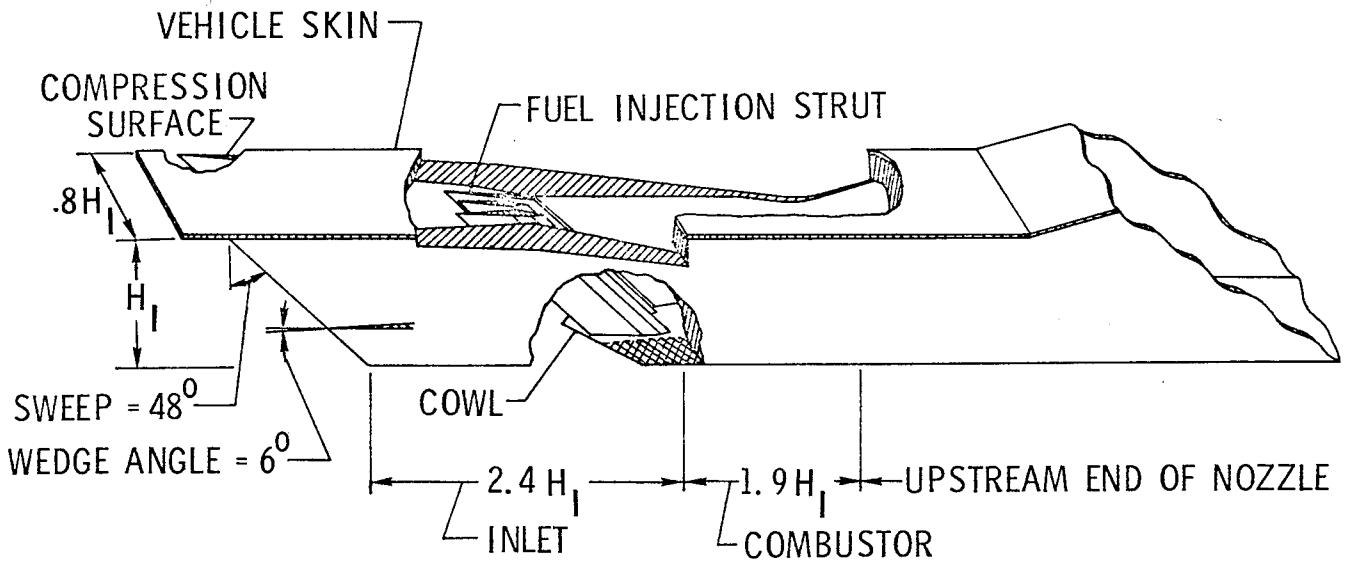

Figure 15.- Langley scramjet concept. Oblique view of inner module.

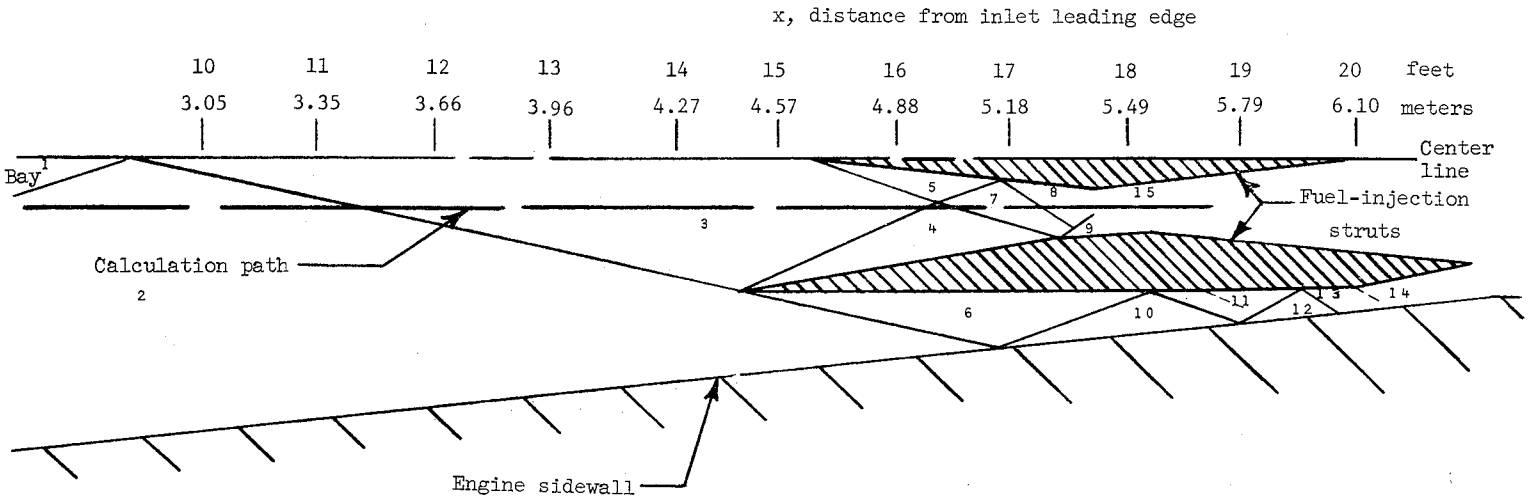

Bay	M	Bay	M
1	5.0	9	2.69
2	4.39	10	3.51
3	3.91	11	3.18
4	3.26	12	2.89
5	3.64	13	2.62
6	3.91	14	2.50
7	3.00	15	2.39
8	2.58		

(a) $M_\infty = 6.07$.

Figure 16.- Inlet shock diagrams.

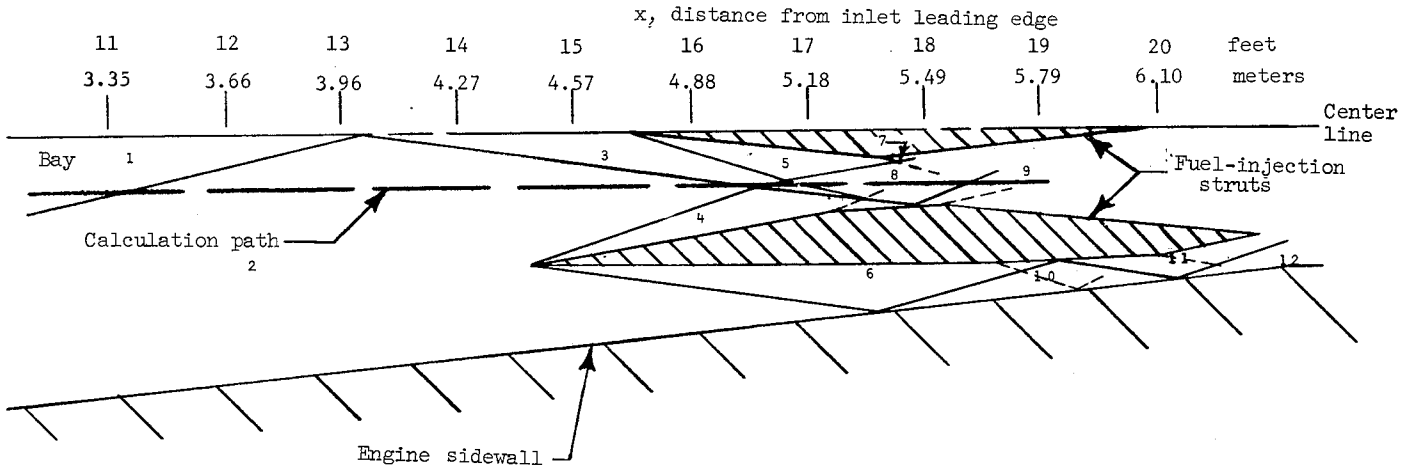

Bay	M	Bay	M
1	7.00	8	4.33
2	5.96	9	3.94
3	5.21	10	4.64
4	5.45	11	4.35
5	4.64	12	4.08
6	5.21		
7	4.82		

(b) $M_\infty = 9.22$.

Figure 16.- Concluded.

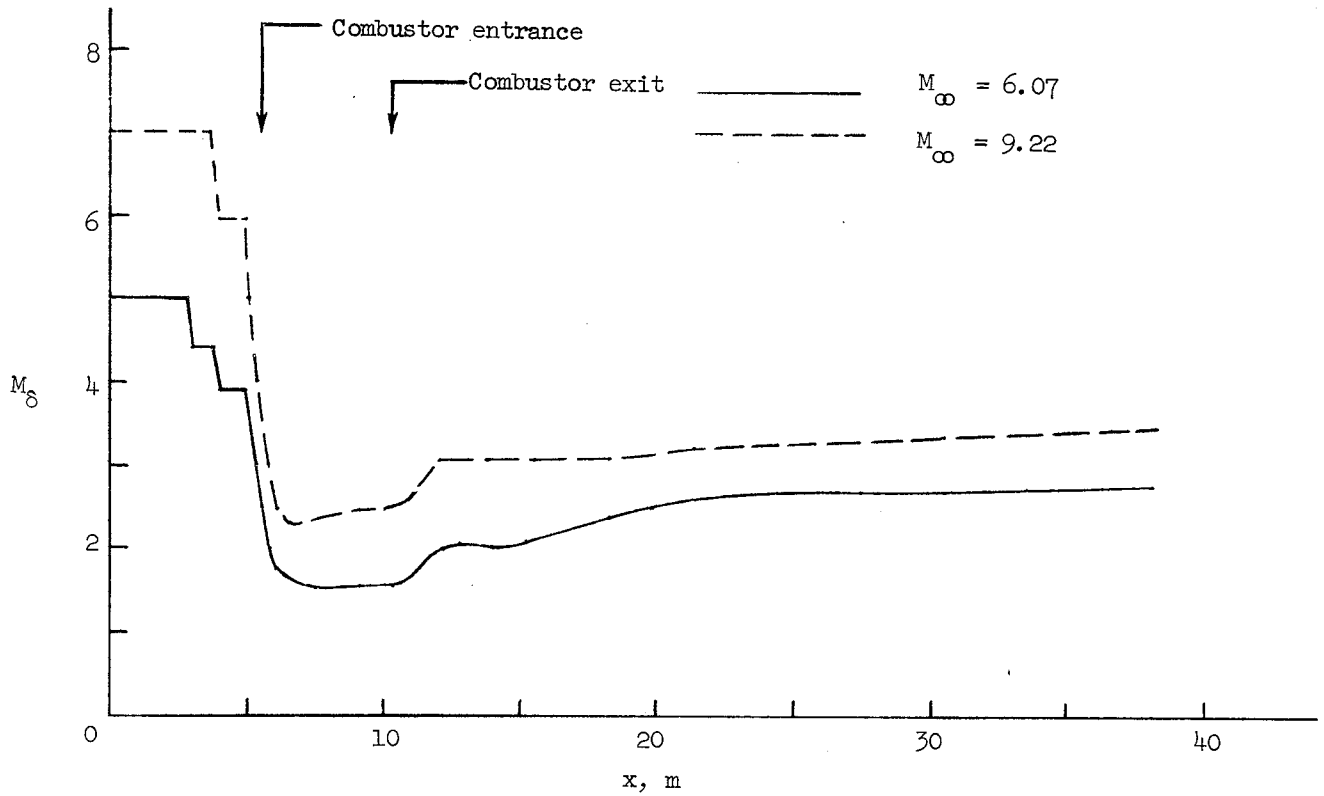

(a) Mach number.

Figure 17.- Boundary-layer edge conditions. Top surface.

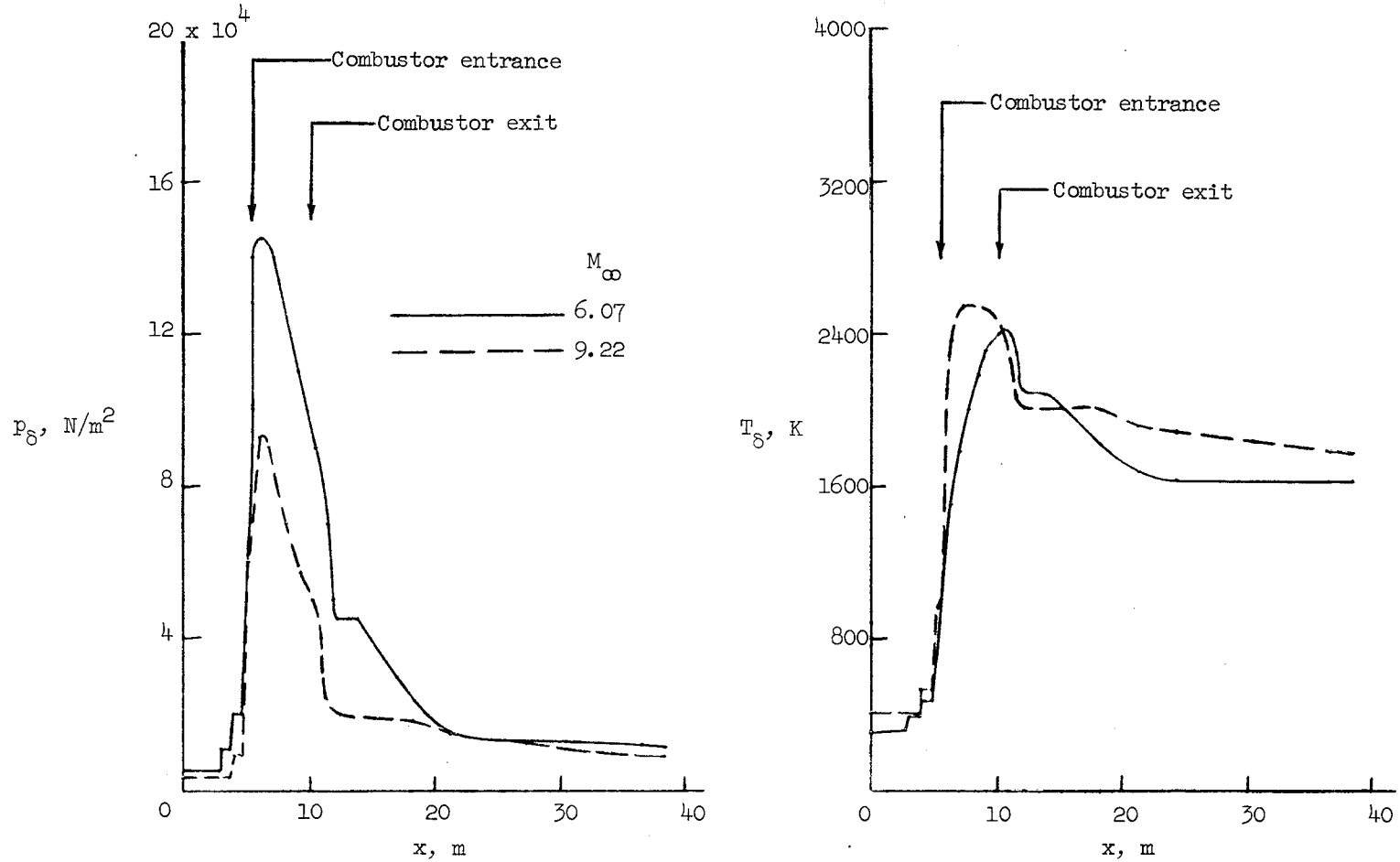

(b) Static pressure and temperature.

Figure 17.- Concluded.

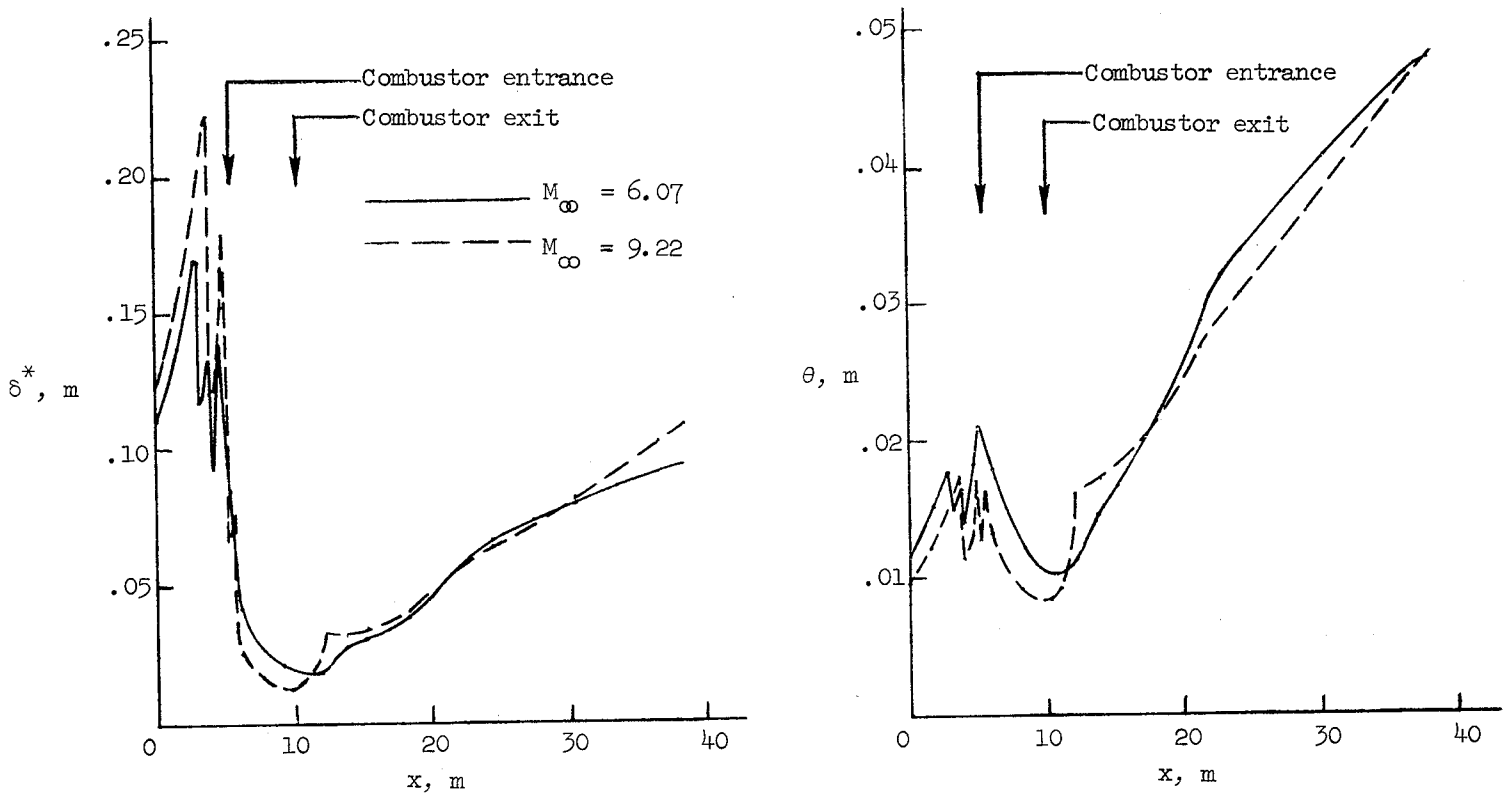

Figure 18.- Predicted boundary-layer growth.

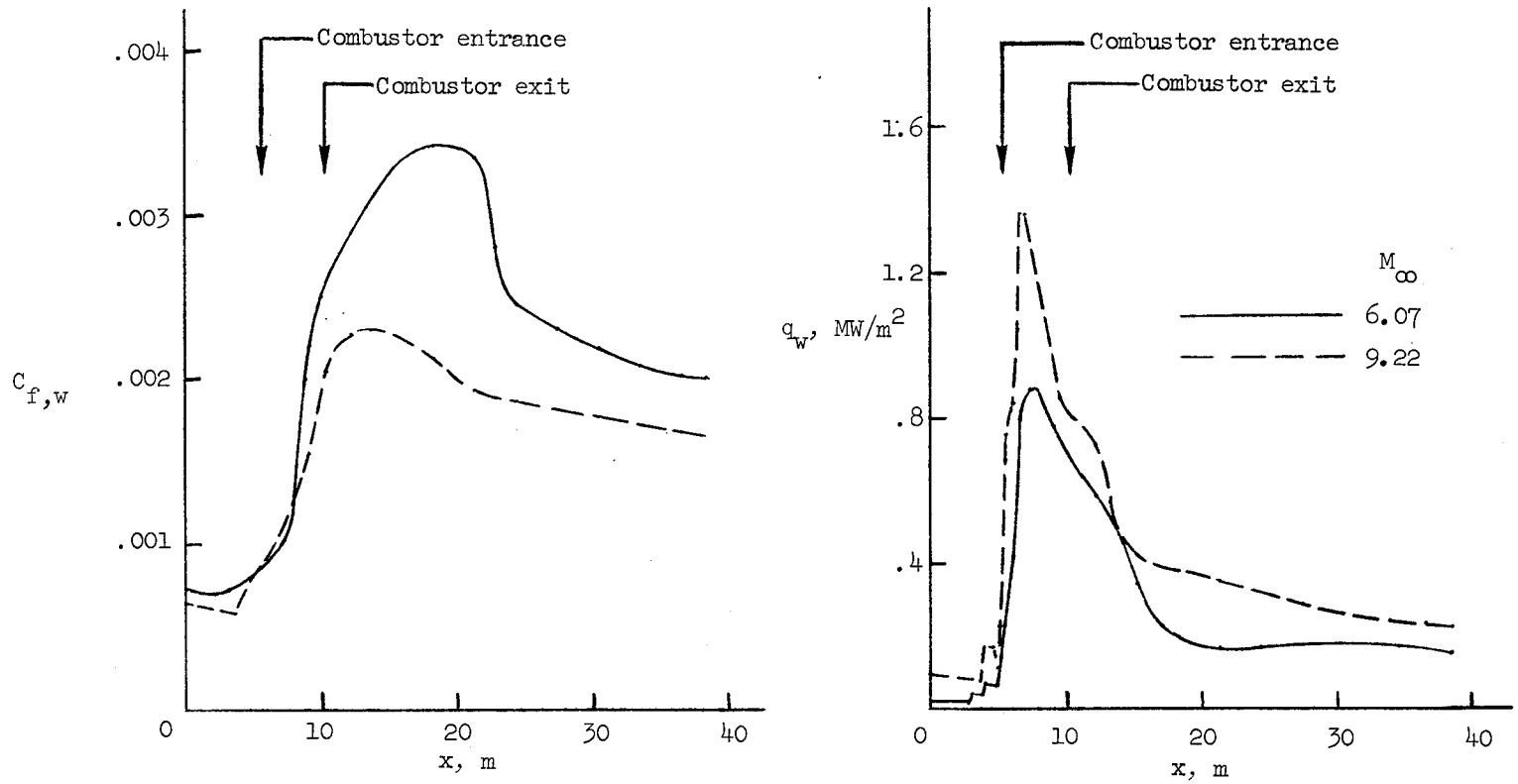

Figure 19.- Predicted friction and heat transfer.

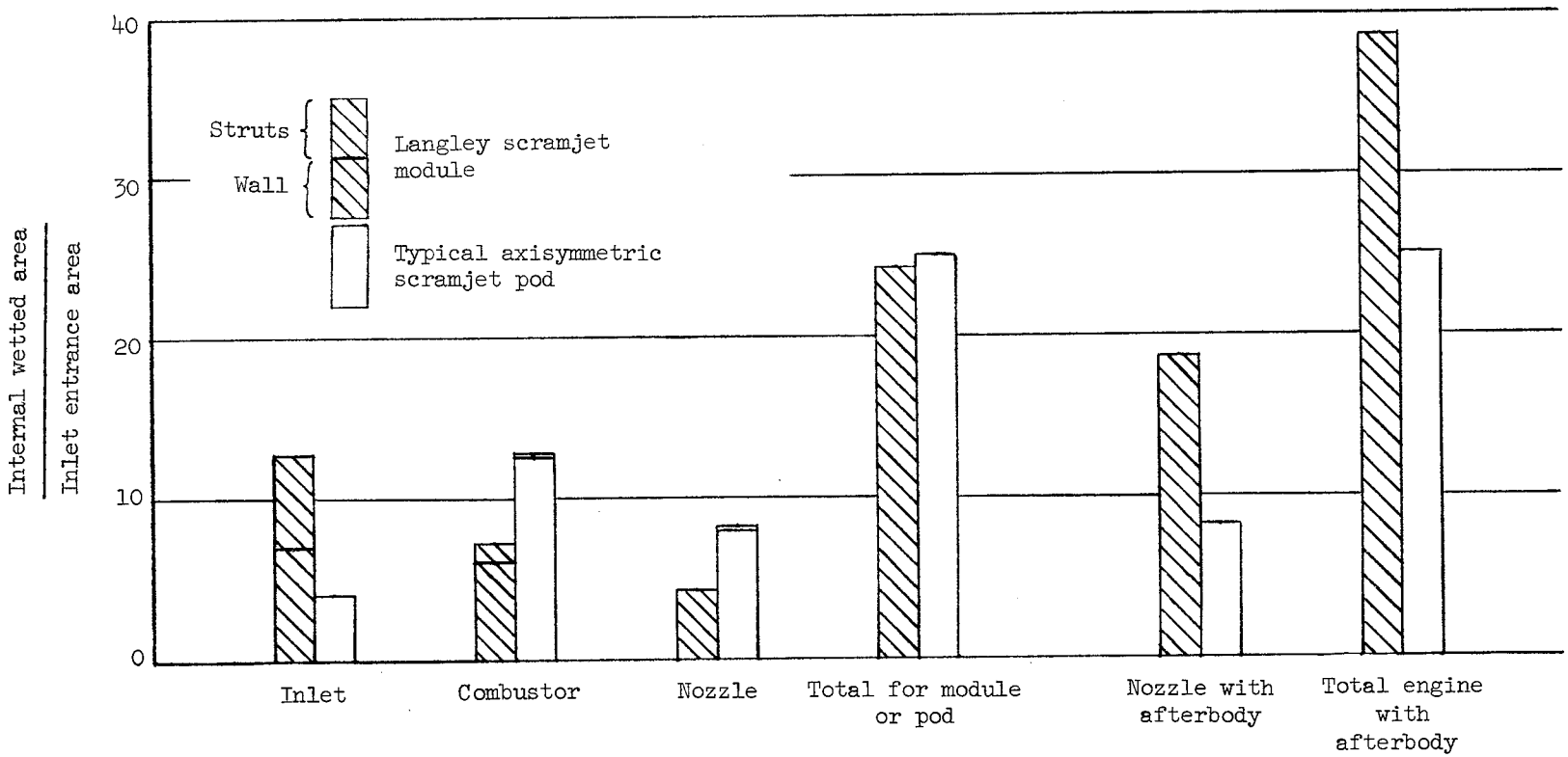

Figure 20.- Scramjet internal wetted surface area.

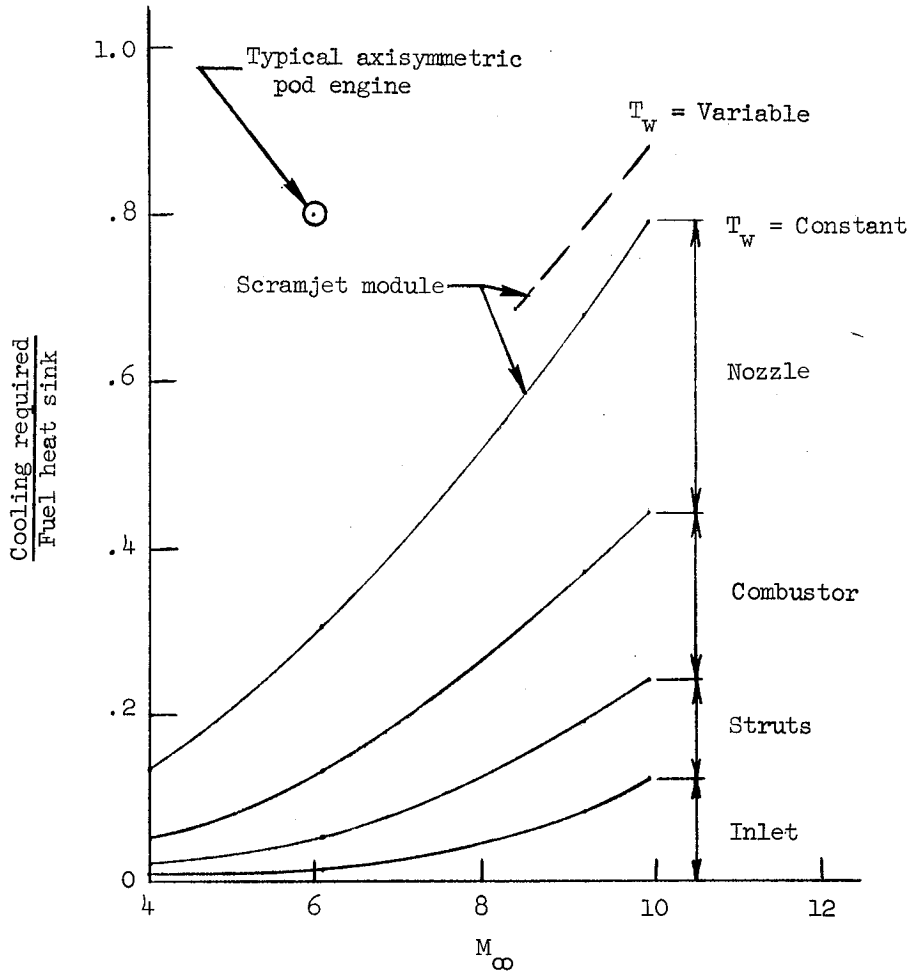

Figure 21.- Langley scramjet cooling requirement. q_∞ = 47.9 kN/m^2 (1000 lb/ft^2); Φ = 1.0.

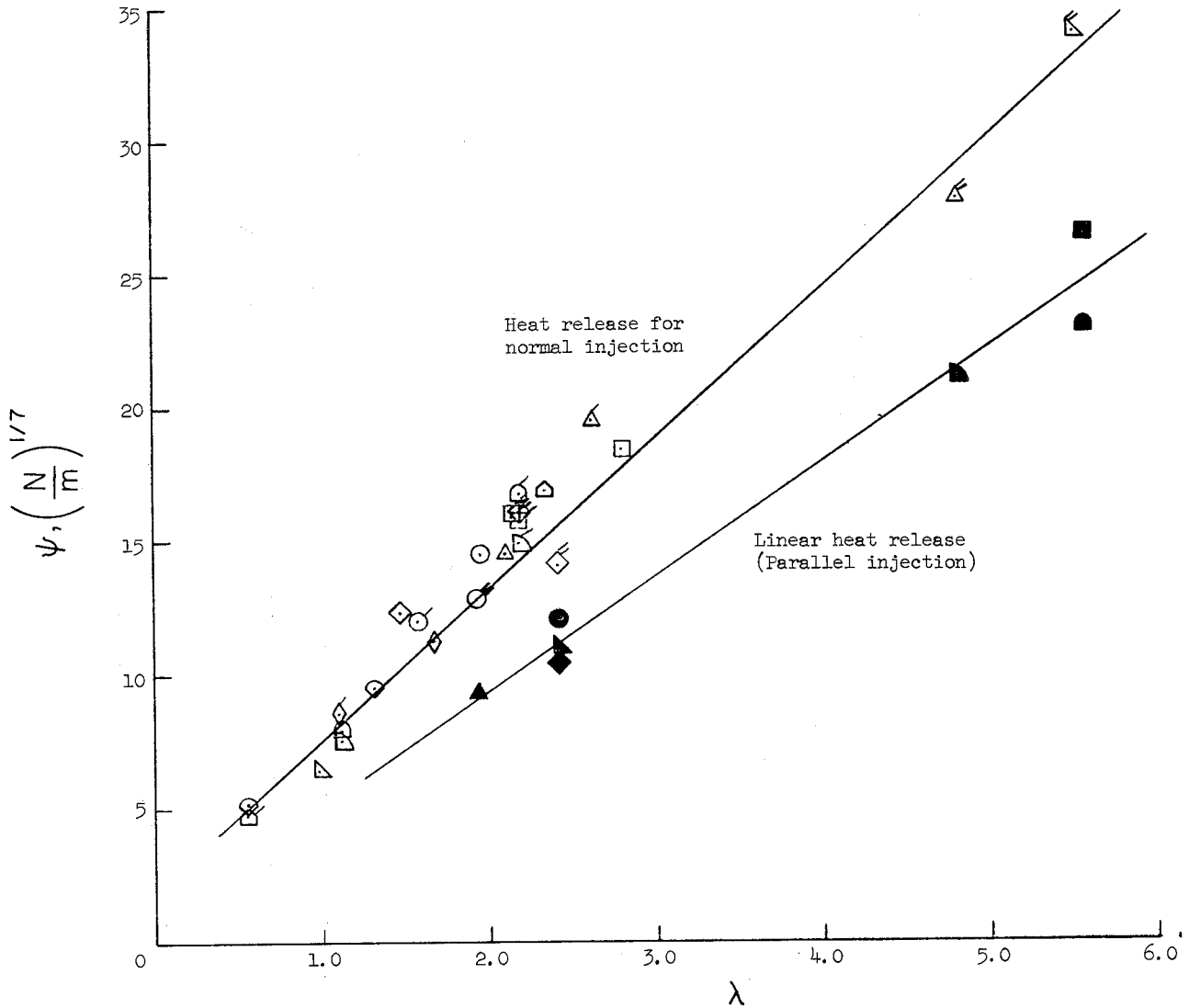

Figure 22.- Correlation for combustor cooling requirements using the hydrogen fuel as a heat sink. See table I for key.